



NAVAL
POSTGRADUATE
SCHOOL

MONTEREY, CALIFORNIA

THESIS

**ATMOSPHERIC TRANSMISSION WINDOWS FOR HIGH
ENERGY SHORT PULSE LASERS**

by

Mun Kit Chan

December 2003

Thesis Advisor:

Donald L. Walters

Co-Advisor:

Alfred W. Cooper

Approved for public release; distribution is unlimited

THIS PAGE INTENTIONALLY LEFT BLANK

REPORT DOCUMENTATION PAGE			Form Approved OMB No. 0704-0188	
Public reporting burden for this collection of information is estimated to average 1 hour per response, including the time for reviewing instruction, searching existing data sources, gathering and maintaining the data needed, and completing and reviewing the collection of information. Send comments regarding this burden estimate or any other aspect of this collection of information, including suggestions for reducing this burden, to Washington headquarters Services, Directorate for Information Operations and Reports, 1215 Jefferson Davis Highway, Suite 1204, Arlington, VA 22202-4302, and to the Office of Management and Budget, Paperwork Reduction Project (0704-0188) Washington DC 20503.				
1. AGENCY USE ONLY (Leave blank)		2. REPORT DATE December 2003	3. REPORT TYPE AND DATES COVERED Master's Thesis	
4. TITLE AND SUBTITLE: Atmospheric Transmission Windows for High Energy Short Pulse Lasers			5. FUNDING NUMBERS	
6. AUTHOR(S) Mun Kit Chan				
7. PERFORMING ORGANIZATION NAME(S) AND ADDRESS(ES) Naval Postgraduate School Monterey, CA 93943-5000			8. PERFORMING ORGANIZATION REPORT NUMBER	
9. SPONSORING /MONITORING AGENCY NAME(S) AND ADDRESS(ES) N/A			10. SPONSORING/MONITORING AGENCY REPORT NUMBER	
11. SUPPLEMENTARY NOTES The views expressed in this thesis are those of the author and do not reflect the official policy or position of the Department of Defense or the U.S. Government.				
12a. DISTRIBUTION / AVAILABILITY STATEMENT Approved for public release; distribution is unlimited			12b. DISTRIBUTION CODE	
13. ABSTRACT (maximum 200 words) The US Navy is exploring the feasibility of using a high energy laser weapon as a ship-borne self-defense system against sea-skimming cruise missile attacks. Since the attenuation of laser energy by the atmosphere is the highest at low altitudes and varies with frequency, the selection of appropriate wavelengths becomes critical for a laser weapon to be effective. A high energy free electron laser (FEL) is suitable for employment in the envisaged role because it can be designed to operate at any desired frequency and, to a degree, is tunable in operation. This study aims to determine the optimal atmospheric windows for high energy, pico second, short pulse lasers. Computer simulations were carried out by convolving a pulse spectrum with the transmission spectrum and the absorption coefficient from the MODTRAN and FASCODE atmospheric codes. Transmission spectrum and absorption coefficient plots were compared to find the range of suitable wavelengths that give good transmittance and low absorption coefficient values. The molecular absorption spectrum was chosen over the extinction spectrum because of known limitations of the Navy Aerosol Model results incorporated into the MODTRAN and FASCODE calculations. Results showed that several suitable windows could be found within the 0.95 to 2.5 μm region that offer at least 90% transmittance with absorption coefficient values of not more than 0.02 per km. For 99% transmittance, optimal wavelengths are between 1.03 and 1.06 μm , and around 1.241 and 1.624 μm . However, the disadvantage of operating near the 1 μm region is the high aerosol extinction. The Navy Aerosol Model used in the atmospheric codes needs to be validated or replaced and actual aerosol data collected in the geographical areas of interest before a more accurate assessment of the optimal wavelengths can be made				
14. SUBJECT TERMS Atmospheric Transmission Spectrum, Optimal Wavelengths for Transmission of High Energy Lasers, MODTRAN and FASCODE Atmospheric Codes, Absorption Coefficient, Free Electron Laser.			15. NUMBER OF PAGES 93	
			16. PRICE CODE	
17. SECURITY CLASSIFICATION OF REPORT Unclassified	18. SECURITY CLASSIFICATION OF THIS PAGE Unclassified	19. SECURITY CLASSIFICATION OF ABSTRACT Unclassified	20. LIMITATION OF ABSTRACT UL	

NSN 7540-01-280-5500

Standard Form 298 (Rev. 2-89)
Prescribed by ANSI Std. Z39-18

THIS PAGE INTENTIONALLY LEFT BLANK

Approved for public release; distribution is unlimited

ATMOSPHERIC WINDOWS FOR HIGH ENERGY SHORT PULSE LASERS

Mun Kit Chan
Lieutenant Colonel, Republic of Singapore Air Force
B.Eng.(Hons), University of London, 1989

Submitted in partial fulfillment of the
requirements for the degree of

MASTER OF SCIENCE IN COMBAT SYSTEMS TECHNOLOGY

from the

**NAVAL POSTGRADUATE SCHOOL
December 2003**

Author: Mun Kit Chan

Approved by: Prof Donald L. Walters
Thesis Advisor

Prof Alfred W. Cooper
Co-Advisor

Prof James H. Luscombe
Chairman, Department of Physics

THIS PAGE INTENTIONALLY LEFT BLANK

ABSTRACT

The US Navy is exploring the feasibility of using a high energy laser weapon as a ship-borne self-defense system against sea-skimming cruise missile attacks. Since the attenuation of laser energy by the atmosphere is the highest at low altitudes and varies with frequency, the selection of appropriate wavelengths becomes critical for a laser weapon to be effective. A high energy free electron laser (FEL) is suitable for employment in the envisaged role because it can be designed to operate at any desired frequency and, to a degree, is tunable in operation. This study aims to determine the optimal atmospheric windows for high energy, pico second, short pulse lasers. Computer simulations were carried out by convolving a pulse spectrum with the transmission spectrum and the absorption coefficient from the MODTRAN and FASCODE atmospheric codes. Transmission spectrum and absorption coefficient plots were compared to find the range of suitable wavelengths that give good transmittance and low absorption coefficient values. The molecular absorption spectrum was chosen over the extinction spectrum because of known limitations of the Navy Aerosol Model results incorporated into the MODTRAN and FASCODE calculations. Results showed that several suitable windows could be found within the 0.95 to 2.5 μm region that offer at least 90% transmittance with absorption coefficient values of not more than 0.02 per km. For 99% transmittance, optimal wavelengths are between 1.03 and 1.06 μm , and around 1.241 and 1.624 μm . However, the disadvantage of operating near the 1 μm region is the high aerosol extinction. The Navy Aerosol Model used in the atmospheric codes needs to be validated or replaced and actual aerosol data collected in the geographical areas of interest before a more accurate assessment of the optimal wavelengths can be made.

THIS PAGE INTENTIONALLY LEFT BLANK

TABLE OF CONTENTS

I.	INTRODUCTION.....	1
A.	EMPLOYMENT OF HIGH-ENERGY LASERS	1
B.	ATTRIBUTES OF LASER WEAPON SYSTEMS.....	2
1.	Speed-of-light Response.....	2
2.	Fast Maneuvering and Crossing Targets.....	3
3.	Deep Magazine.....	3
4.	Minimal Collateral Damage	3
5.	Target Identification	4
6.	Lethal to Non-lethal Employment.....	4
C.	CLASSES OF HIGH ENERGY LASERS	4
1.	Chemical Lasers	4
2.	Solid-state Lasers.....	5
3.	Free Electron Lasers	6
D.	ISSUES ASSOCIATED WITH SHIP-BASED LASER SYSTEMS	7
E.	OUTLINE OF THESIS.....	8
II.	ATMOSPHERIC EFFECTS ON LASER TRANSMISSION	11
A.	INTRODUCTION.....	11
B.	THE ATMOSPHERE	11
C.	GAS COMPOSITION	12
D.	PARTICLE COMPOSITION	14
E.	ATMOSPHERIC EFFECTS.....	15
F.	ABSORPTION SPECTRAL LINE-SHAPE.....	19
G.	MOLECULAR ABSORPTION BY ATMOSPHERIC GASES.....	20
H.	SCATTERING OF RADIATION	22
I.	THERMAL BLOOMING OF HIGH POWER LASER RADIATION	24
III.	COMPUTER MODELS FOR ATMOSPHERIC TRANSMISSION	27
A.	LOWTRAN	28
B.	MODTRAN	30
C.	HITRAN.....	31
D.	FASCODE.....	31
IV.	SIMULATION ANALYSIS.....	33
A.	INTRODUCTION.....	33
B.	EFFECTS OF THE LASER PULSE WIDTH ON THE TRANSMISSION SPECTRUM.....	34
C.	MODTRAN INPUT PARAMETERS	36
D.	MODTRAN RUN RESULTS.....	37
1.	Effects of Different Path Lengths	39
2.	Effects of Different Visibility Conditions	40
3.	Seasonal Effects	41
4.	Effects due to Different Pulse Widths	42

5.	Compare Different Regions	42
E.	FASCODE RUN RESULTS	43
F.	ABSORPTION COEFFICIENT SPECTRUM.....	45
1.	Absorption Coefficients for Existing High Energy Lasers .	52
G.	OPTIMAL WAVELENGTH BANDS	55
H.	MODTRAN AND FASCODE CONSISTENCY	62
I.	EFFECTS OF LONGER PULSE WIDTHS.....	65
V.	CONCLUSIONS AND RECOMMENDATIONS.....	69
A.	CONCLUSIONS.....	69
1.	MODTRAN Results	70
2.	FASCODE Results	71
B.	RECOMMENDATIONS FOR FURTHER WORK.....	71
	LIST OF REFERENCES.....	73
	INITIAL DISTRIBUTION LIST	75

LIST OF FIGURES

Figure 1.	Structure of the Earth's Atmosphere.....	12
Figure 2.	Low-resolution solar spectrum compared with laboratory spectra of atmospheric gases. (From [Ref. 5]).	14
Figure 3.	Atmospheric Transmittance as a function of wavelength. (From [Ref. 7]).	17
Figure 4.	Absorption coefficient of a spectral line, where $\nu_0 = (E_1 - E_0)/hc = f_0/c$, where c is the speed of light. (From [Ref. 4]).	20
Figure 5.	Comparison of normalized Gaussian and Lorentzian curves.	21
Figure 6.	Spreading of laser beam passing through a negative lens.	26
Figure 7.	Free Electron Pulse waveform.	34
Figure 8.	Plot of normalized function $G(f)$	36
Figure 9.	Atmospheric transmission spectrum using MODTRAN for a 10 km long, 10 m high path with 50 km visibility for Korea on 1 Jan.	38
Figure 10.	Transmission spectrum for a 1 ps FEL Gaussian pulse using MODTRAN for a 10 km long, 10 m high path with 50 km visibility for Korea on 1 Jan.	38
Figure 11.	Transmission spectra for a 1 ps FEL Gaussian pulse using MODTRAN for 2 and 10 km long, 10 m high paths with a 50 km visibility for Korea on 1 Jan.....	39
Figure 12.	Atmospheric transmission spectra for a 1 ps FEL Gaussian pulse using MODTRAN for 2 km long, 10 m high path with 1, 5, 23 and 50 km visibility for Korea on 1 Jan.....	40
Figure 13.	Atmospheric transmission spectra for a 1 ps FEL Gaussian pulse using MODTRAN for a 10 km long, 10 m high path with 50 km visibility for Korea on 1 Jan and 1 July.	41
Figure 14.	Atmospheric transmission spectra for 0.25 and 1 ps FEL Gaussian pulses using MODTRAN for a 10 km long, 10 m high path for Korea on 1 Jan.....	42
Figure 15.	Atmospheric transmission spectra for a 1 ps FEL Gaussian pulse using MODTRAN for a 10 km long, 10 m high path with 50 km visibility for Korea, Persian Gulf and Taiwan on 1 Jan.....	43
Figure 16.	Suitable atmospheric transmission windows for a 1 ps FEL Gaussian pulse.....	44
Figure 17.	Atmospheric transmission spectrum using FASCODE for a 10 km long, 10 m high path with 50 km visibility for Korea on 1 Jan.	47
Figure 18.	Molecular transmission spectrum using FASCODE for a 10 km long, 10 m high path for Korea on 1 Jan.....	47
Figure 19.	Molecular transmission for a 1 ps FEL Gaussian pulse using FASCODE for a 10 km long, 10 m high path for Korea on 1 Jan.....	48
Figure 20.	Absorption coefficient using FASCODE for a 10 km long, 10 m high path for Korea on 1 Jan.....	48

Figure 21.	Absorption coefficient from 1.51 to 1.73 μm using FASCODE for a 10 km long, 10 m high path for Korea on 1 Jan.....	50
Figure 22.	FASCODE absorption coefficients convolved with 1 ps Gaussian pulse for a 10 km long, 10 m high path with 50 km visibility for Korea on 1 Jan.	50
Figure 23.	FASCODE absorption coefficients from 1.635 to 1.666 μm for a 10 km long, 10 m high path for Korea on 1 Jan.....	51
Figure 24.	FASCODE extinction coefficient from 1.635 to 1.666 μm for a 10 km long, 10 m high path for Korea on 1 Jan.....	51
Figure 25.	Absorption coefficient near the of Nd Yag laser operating wavelength.	52
Figure 26.	Absorption coefficient near the oxygen-iodine laser operating wavelength.	53
Figure 27.	Absorption coefficient near the P(8) and P(9) deuterium fluoride laser operating wavelengths. [Ref. 15].	53
Figure 28.	Absorption coefficient near the P(10) and P(11) deuterium fluoride laser operating wavelengths. [Ref. 15].	54
Figure 29.	Absorption coefficient near the P(12) and P(13) deuterium fluoride laser operating wavelengths. [Ref. 15].	54
Figure 30.	Molecular transmission for a 1 ps FEL Gaussian pulse from 0.95 to 1.11 μm using FASCODE for a 10 km long, 10 m high path for Korea on 1 Jan and 1 July.....	57
Figure 31.	Absorption coefficient for a 1 ps FEL Gaussian pulse from 0.95 to 1.11 μm using FASCODE for a 10 km long, 10 m high path for Korea on 1 Jan and 1 July.....	57
Figure 32.	Molecular transmission for a 1 ps FEL Gaussian pulse from 1.11 to 1.33 μm using FASCODE for a 10 km long, 10 m high path for Korea on 1 Jan and 1 July.....	58
Figure 33.	Absorption coefficient for a 1 ps FEL Gaussian pulse from 1.11 to 1.33 μm using FASCODE for a 10 km long, 10 m high path for Korea on 1 Jan and 1 July.....	58
Figure 34.	Molecular transmission for a 1 ps FEL Gaussian pulse from 1.47 to 1.82 μm using FASCODE for a 10 km long, 10 m high path for Korea on 1 Jan and 1 July.....	59
Figure 35.	Absorption coefficient for a 1 ps FEL Gaussian pulse from 1.47 to 1.82 μm using FASCODE for a 10 km long, 10 m high path for Korea on 1 Jan and 1 July.....	59
Figure 36.	Molecular transmission for a 1 ps FEL Gaussian pulse from 2 to 2.5 μm using FASCODE for a 10 km long, 10 m high path for Korea on 1 Jan and 1 July.	60
Figure 37.	Absorption coefficient for a 1 ps FEL Gaussian pulse from 2 to 2.5 μm using FASCODE for a 10 km long, 10 m high path for Korea on 1 Jan and 1 July.	60

Figure 38.	Molecular transmission for a 1 ps FEL Gaussian pulse from 3.45 to 4.16 μm using FASCODE for a 10 km long, 10 m high path for Korea on 1 Jan and 1 July.....	61
Figure 39.	Absorption coefficient for a 1 ps FEL Gaussian pulse from 3.45 to 4.16 μm using FASCODE for a 10 km long, 10 m high path for Korea on 1 Jan and 1 July.....	61
Figure 40.	FASCODE and MODTRAN spectra for a 1 ps FEL Gaussian pulse from 0.95 to 1.12 μm for a 10 km long, 10 m high path with 50 km visibility for Korea on 1 Jan.....	62
Figure 41.	FASCODE and MODTRAN spectra for a 1 ps FEL Gaussian pulse from 1.1 to 1.35 μm for a 10 km long, 10 m high path with 50 km visibility for Korea on 1 Jan.....	63
Figure 42.	FASCODE and MODTRAN spectra for a 1 ps FEL Gaussian pulse from 1.4 to 1.85 μm for a 10 km long, 10 m high path with 50 km visibility for Korea on 1 Jan.....	63
Figure 43.	FASCODE and MODTRAN spectra for a 1 ps FEL Gaussian pulse from 2 to 2.5 μm for a 10 km long, 10 m high path with 50 km visibility for Korea on 1 Jan.....	64
Figure 44.	FASCODE and MODTRAN spectra for a 1 ps FEL Gaussian pulse from 3.45 to 4.2 μm for a 10 km long, 10 m high path with 50 km visibility for Korea on 1 Jan.....	64
Figure 45.	Atmospheric extinction spectra between 1.1 and 1.35 μm for 1 ps and 2 ps Gaussian pulses for a 10 km long, 10 m high path for Korea on 1 Jan.	65
Figure 46.	Atmospheric extinction spectra between 1.1 and 1.35 μm for 1 ps and 5 ps Gaussian pulses for a 10 km long, 10 m high path for Korea on 1 Jan.	66
Figure 47.	Atmospheric extinction spectra between 1.1 and 1.35 μm for 1 ps and 10 ps Gaussian pulses for a 10 km long, 10 m high path for Korea on 1 Jan.	66
Figure 48.	FASCODE absorption coefficients convolved with 1 and 2 ps Gaussian pulses for a 10 km long, 10 m high path for Korea on 1 Jan.....	67
Figure 49.	FASCODE absorption coefficients convolved with 1 and 5 ps Gaussian pulses for a 10 km long, 10 m high path for Korea on 1 Jan.....	68
Figure 50.	FASCODE absorption coefficients convolved with 1 and 10 ps Gaussian pulses for a 10 km long, 10 m high path for Korea on 1 Jan.....	68

THIS PAGE INTENTIONALLY LEFT BLANK

LIST OF TABLES

Table 1.	Gases Present in Standard Amounts in a Dry Atmosphere. (After [Ref. 4]).....	13
Table 2.	Order of Significance of Attenuation Coefficients. (From [Ref. 6]).	18
Table 3.	Particles responsible for atmospheric scattering. (From [Ref. 4]).	23
Table 4.	Atmospheric and aerosol models for LOWTRAN. (From [Ref. 9]).	29
Table 5.	Summary of suitable wavelength bands for FEL operation for a 10 km horizontal path, 10 m above the ocean with no aerosol extinction.	56

THIS PAGE INTENTIONALLY LEFT BLANK

ACKNOWLEDGMENTS

I would first like to express my appreciation to Professor Donald Walters to whom I am especially grateful for his guidance and assistance throughout this project. I also want to thank Professor Cooper for his advice and support. Finally I would like to thank my lovely wife Josephine, and my three wonderful children, Leonard, Elaine and Ryan, for their understanding, encouragement and steadfast support without which I would not be able to complete my program in NPS successfully.

THIS PAGE INTENTIONALLY LEFT BLANK

I. INTRODUCTION

A. EMPLOYMENT OF HIGH-ENERGY LASERS

The research and development of high-energy laser (HEL) and other directed energy concepts such as particle beams and high-power microwaves by the US military has waxed and waned during the last 30 years. In the 1970s, the services were highly interested in HELs as an alternative to conventional guns and missiles. The United States Navy's mission of interest was, and still is, shipboard defense against maneuvering low-altitude cruise missiles that could saturate the Phalanx gun system. The Navy developed the MIRACL chemical laser system for ship defense against cruise missiles in the early 1980s; however, the size, weight, toxic chemicals, and long wavelength caused the Navy to lose interest in HEL. [Ref. 1]. A laser beam delivers its energy either in a continuous wave mode (CW) or in a pulsed mode to a relatively small spot on the target. The beam aims at specific points of the target's body that are known to be vulnerable such as fuel tanks and aerodynamic control surfaces of a missile. Irradiance in the 10^3 to 10^4 KW/cm² range can be sufficient to melt through a missile body in a few seconds. Moreover, if the heated area is under stress (aerodynamic or static pressure load), the lethal effects to the target system occur more quickly.

With recent advances in laser technology, defense planners are taking a fresh look at HEL weapon systems. The HEL could also be a weapon of choice for a transformational military concerned with homeland defense, asymmetric threats from rogue powers and terrorists, and urban warfare, as well as the more traditional military missions on the battlefield and at sea. It has the potential to address a range of applications and missions from ground to space. The potential missions include ballistic missile defense, air defense, attack against ground and maritime targets, maritime self-defense, space control, urban operations, clearance of exposed mines, surveillance and counter-surveillance.

The platforms on which the HELs can be deployed include ships, large or tactical aircraft including helicopters, ground vehicles, ground bases and spacecraft. Longstanding missions such as ship self-defense are under investigation to determine if advances in both HEL technology and electric on-board power, compared to advances in the threat capability coupled with new threat scenarios, have tilted the development of future ship systems defense to favor HEL weapons.

B. ATTRIBUTES OF LASER WEAPON SYSTEMS

The HEL has the key attributes of speed-of-light response, ability to handle fast maneuvering and crossing targets, deep magazine capacity, minimal collateral damage, target identification and adaptability for lethal to non-lethal employment.

1. Speed-of-light Response

The principle attribute of HEL is speed-of-light delivery of energy. A good illustration of this attribute is to consider the typical timings available for the engagement of a target compared with the flight time of projectiles and missiles. In the context of naval operations, there is a need to defend against an incoming sea-skimming supersonic cruise missile flying only a few feet above the top of the waves. If the threat is detected as it comes over the horizon, about 15 miles out, and is traveling at Mach 3, the time from detection to impact will last approximately 24 seconds only. The ship's defense problem could be compounded if several simultaneous high-speed missiles are fired at it, and its defensive system would be overwhelmed even if several defensive missiles are fired at the same time. Laser travels at the speed of light and can be focused into a narrow beam for propagation. Hence, HELs are extremely fast and very precise. HEL can be activated to begin their attack within seconds of the target's detection and complete its destruction a few seconds later. This enables them to execute multiple shots in order to destroy the target or engage multiple targets.

2. Fast Maneuvering and Crossing Targets

If the same cruise missile scenario outlined above concerned a maneuvering target, the gun or missile kill would be greatly complicated since a defensive missile typically needs a three-to-one gravity (G) advantage over the target. A maneuvering target, however, is probably even more vulnerable to an HEL. A weaving target traveling at Mach 3 and executing 20+Gs will be much more susceptible to breakup after being damaged by the laser. A crossing target also presents its side profile rather than just its nose to the HEL beam, thereby increasing the target's vulnerability to a guidance or propellant kill.

3. Deep Magazine

The magazine for an HEL is laser-reactant fuel for a chemical laser, or electric generator fuel for both solid-state lasers and free-electron lasers. The lasers can run as long as fuel is available, which provides for a very deep magazine. Another plus point is that the power needed to run an electric HEL and the power necessary to propel a surface combatant can be the same, particularly on the new all-electric ship concepts. This means that fuel is available for hours of HEL run time. The number of simultaneous targets that can be engaged depends on the hardness of the target and the irradiance time needed for a kill, typically several seconds. In a ship defense scenario, two or three simultaneous threats might be engaged sequentially before engagement time runs out. If the threats are spaced sufficiently, only fuel or electric power limits the number of engagements.

4. Minimal Collateral Damage

The precision pointing and tracking of the beam director leads to lower collateral damage. For example, consider air defense in an urban environment. An air defense projectile or missile that does not engage a target, unless it has the ability to self-destruct, provides a real threat to people and dwellings on the ground. In contrast, an HEL does not produce unexpended rounds, and there is

no additional ground threat. This attribute might make an HEL attractive for the defense of high-value buildings and facilities.

5. Target Identification

The HEL beam director is a high-quality telescope using reflecting optics that can provide a detailed image of the target. While the reflective coatings on the mirrors are tuned to the frequency of the HEL, there is residual reflectivity at other wavelengths, including the visible. This imagery can be used to provide a positive identification of the target.

6. Lethal to Non-lethal Employment

The power output of a laser can be modulated from destruction at full power, to disable at lower power, to deny and dissuade at even lower power. A low-power laser could be deployed to warn away potential threats and to destroy or blind threat sensors. The Navy has looked at reducing the power of an HEL for use at sea as a warning device to approaching small craft. At higher laser powers, the craft, such as a speedboat or a jet ski watercraft, could be damaged or destroyed (a difficult task for a 5-inch gun).

C. CLASSES OF HIGH ENERGY LASERS

There are three classes of HEL currently under development: chemical lasers, solid-state lasers, and free-electron lasers. Work on other types of HELs, such as the gas dynamic laser and the pulsed electric gas discharge laser, was discontinued years ago because the lasers produced beams at unfavorable wavelengths for propagation.

1. Chemical Lasers

Chemical lasers produce radiation from excited atomic or molecular species resulting from chemical reactions. Weapon class chemical lasers include hydrogen and deuterium fluoride (HF and DF) and chemical oxygen/iodine lasers

(COIL). These devices have achieved megawatt power levels with good beam quality. The MIRACL is a deuterium fluoride (DF) laser operating at a set of wavelengths around 3.8 microns that has been in continuous operation at the megawatt level since the mid 1980s at the White Sands HEL Systems Test Facility. It was originally conceived as a test bed for ship self-defense but suffered from propagation losses at full power. The hydrogen fluoride (HF) laser is similar to the DF laser but operates at a shorter wavelength (2.7 microns), which will not propagate well in the atmosphere but will perform well in space, potentially for ballistic missile defense. The Navy discontinued the development of chemical lasers because of their inherent propagation losses in the operational wavelengths. [Ref. 1].

2. Solid-state Lasers

Solid-state lasers (SSLs) produce radiation from excited atomic or ionic species of a solid-state material. The atomic excitation is achieved by providing a power supply to the solid-state material. SSLs have the most potential for a compact engineered weapon, although current devices are still large and complex. The laser does not require flowing exotic gases or relativistic electron beams. The system could be inherently smaller and less complex than the other laser concepts. The lasers also operate at about 1.06 microns, lower wavelengths than the COIL, which further simplifies the optics. However, SSLs have the largest challenge to scale up to megawatt power levels because of waste heat removal. Waste heat from a chemical laser is carried off in the flowing gas medium. The unexpended energy in the electron beam of a free-electron laser can be disposed of in a large heat sink. But with a solid-state laser, the waste heat remains in the laser medium, increasing the temperature in the medium until lasing with acceptable beam quality is impossible. Several techniques to combat this problem are being studied. The current options are short pulses followed by cool-down, cooled geometries, including fiber-optic laser bundles, and slab lasers. Increasing laser efficiency will also reduce the amount of waste heat. Combining the power output of many smaller lasers into a single

high-power coherent beam has also been investigated. With this concept, some of the system simplicity advantages would be lost. However, the fiber-optic laser successfully uses the principle of beam combination.

A final important technology area for SSLs is the development of affordable, high-power laser diodes to pump the laser to the excited state necessary for lasing. For example, a half-megawatt laser that is 20 percent efficient using 10-watt diodes will require 250,000 pump diodes. With diodes costing more than \$100 each, the price of the diodes alone would be more than \$25 million. At minimum, costs must be reduced by an order of magnitude. While there is a large industrial market for laser diodes for commercial application, there is as yet no other market for the high-power diodes needed for an HEL.

3. Free Electron Lasers

A free electron laser (FEL) produces radiation by passing a relativistic electron beam through an alternating magnetic field called the wiggler. The spatial variations of the wiggler and the electromagnetic wave combine to produce a beat wave which causes the electron beam to form coherent bunches and give rise to stimulated emission in the forward direction of the electron beam. Electrons from an injector are fed into an accelerator where they are accelerated by an electric field to nearly the speed of light. A common accelerator for generating high-power free-electron lasers is the radio-frequency linear accelerator (r.f. linacs). Laser beams based upon r.f. linacs are composed of a sequence of macropulses (typically of microseconds in duration) each of which consists of a train of shorter pico-second pulses. [Ref. 2].

An FEL could be designed to operate at any desired frequency and, to a degree, is tunable in operation. FELs have been operated over a spectrum ranging from microwaves through visible light. There are plans to extend this range to the ultraviolet as well. At ground level, they might have the best chance of producing a beam that propagates successfully through the relatively dense or

"thick" air. Since the laser beam is produced in a vacuum cavity, the beam quality is excellent. Significant technical challenges exist both to scale the existing kilowatt-class laser beam to megawatt powers and to engineer a laboratory device into a weapon system. Another risk technology area is with the resonator optics needed to extract the light from the resonator electron beam in a practical length. The FEL is the most complex of the three HEL alternatives and most likely is suited only for ground or shipboard use.

D. ISSUES ASSOCIATED WITH SHIP-BASED LASER SYSTEMS

From an operational point of view, a Navy ship might seem an ideal platform for an HEL. Ships are far larger than other platforms, and ship defense against cruise missiles is a clearly defined mission. The current lack of a Navy HEL development program is due to the technical issues of propagation and lethality rather than to operational issues. At this stage, an HEL would have to show advanced performance at an affordable cost through a tradeoff study of alternative systems and missions. Pop-up threats such as small speedboats and jet ski watercraft, as well as cruise missile defense, are valid missions.

Given the electrical power availability on modern navy ships, the FEL and the solid-state laser are logical candidates for maritime HEL weapon systems, even though only the chemical lasers have demonstrated weapon-level powers. A significant advantage of FELs and SSLs is that they do not generate the toxic effluents of chemical lasers. The issue of handling the chemical laser on board is serious since the crew could be harmed and equipment damaged. Another disadvantage is the need for a logistics supply of hazardous and toxic chemicals.

Propagation of a high-energy beam at ground or sea level, where the air is relatively dense, has been the single most limiting factor in the Navy's ability to field a shipborne HEL cruise missile defense system. In space, this problem does not exist and is significantly less for the airborne laser systems at altitude. The

principal loss mechanisms at low altitudes are absorption, scattering and thermal blooming, in which absorbed energy in the air creates a negative lens that defocuses the beam. Increasing the power of the beam increases the energy absorbed and worsens the problem. Thermal blooming is nonlinear; it evolves over a horizontal path that has atmosphere all the way to the target. Therefore, closed loop adaptive optics techniques have not proven effective. To address this problem, the Navy is looking at developing free-electron lasers that can generate wavelengths where absorption and thermal blooming are minimized. [Ref. 3]

E. OUTLINE OF THESIS

The objective of this thesis is to determine the optimal wavelengths for a shipborne tactical high-energy free electron laser system. Taking into account the feasible physical dimensions of the weapon system due to limited space onboard naval ships, a smaller operating wavelength is desired because of beam diffraction and optical aperture size considerations. Hence, the wavelength region for this study was chosen to be within 0.6 to 4.2 μm . Chapter II gives an overview of the theoretical background and discusses the physics behind the attenuation of a laser beam as it is transmitted through the atmosphere. Atmospheric absorption and scattering, thermal blooming and absorption spectral lines are examined in detail.

Chapter III of this thesis gives a brief description of the MODTRAN 4.0 and FASCODE 3 computer programs that are used to run the simulations for the atmospheric transmittance, and calculations of the extinction and atmospheric coefficients. Since the FEL operates by transmitting a series of short pulses of pico-seconds duration, the effect is that the laser energy will not be confined to a pure monochromatic spectral line, but spread over a band of frequencies. To investigate the effect of this spreading of frequency spectrum of the laser pulse, the MODTRAN and FASCODE transmission spectra were modified by convolution with the frequency spectrum representing a single FEL pulse. Further

resolution was done by narrowing the simulation runs to within a selected band of frequencies where atmospheric attenuation is less pronounced to investigate the suitable wavelengths for the propagation of a high energy FEL beam.

Chapter IV discusses the results of simulations for a few regions of interest around the world; namely Korea, Taiwan Straits and Persian Gulf regions. The effects of varying atmospheric conditions due seasonal variations, and differences in transmission paths, visibility conditions and FEL pulse width were also examined.

Chapter V summarizes the results found in this study.

THIS PAGE INTENTIONALLY LEFT BLANK

II. ATMOSPHERIC EFFECTS ON LASER TRANSMISSION

A. INTRODUCTION

The performance of military systems for imaging, target detection, tracking, target designation, warning of missile launch or laser irradiation, optical fuzing, or laser weaponry, depends strongly on the transmission and modification of electromagnetic radiation, and also on the fluctuations in these effects. Transmission of electromagnetic (EM) waves through the atmosphere is subjected to attenuation from refraction, absorption and scattering by the molecular constituents and suspended particles in the atmosphere. This chapter starts with a brief description of the structure of the atmosphere, its natural gas composition and suspended aerosol particles. The total extinction coefficient represents the effects of atmospheric attenuation. To understand the phenomena of atmospheric absorption, a background section on atmospheric spectroscopy is included to explain the concept of local-line shape. Spectroscopy of the atmospheric molecules also determines the dispersion and temperature dependence of the index of refraction of air. Laser energy absorbed by the atmosphere heats up and reduces the index of refraction of air, causing thermal blooming which refracts and severely limits the propagating range of a laser beam.

B. THE ATMOSPHERE

The atmosphere consists of four main horizontal layers, as shown in Fig. 1, containing gases and suspended particles at various temperatures and pressures that vary with altitude and azimuth. The closest layer to the earth's surface is the troposphere, which extends from the ground to approximately 11 km (36,000 ft or 7 miles). The temperature in this layer generally decreases with increasing altitude at the rate of about 6.5 K per km, but variations on this rate

can exist which creates interesting refractive effects. The pressure also drops from one atmosphere at sea level to a few tenths of an atmosphere at the top of this layer.

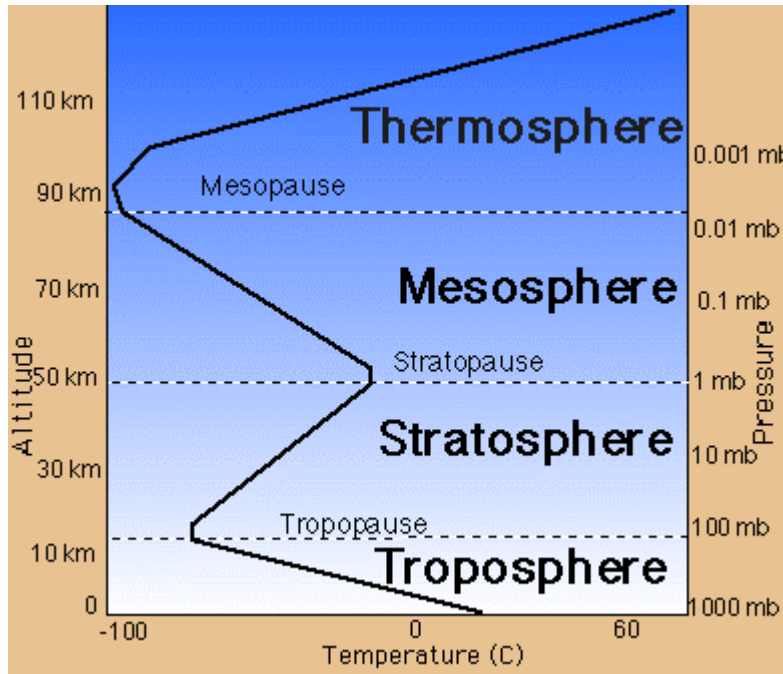


Figure 1. Structure of the Earth's Atmosphere

Most of the important atmospheric attenuators (i.e., H₂O, CO₂, clouds, fog, aerosols in general) exist in the troposphere. Water is most important at lower altitudes, in particular over the ocean as part of the marine boundary layer. For tactical employment of a FEL weapon system by navy ships, we are primarily concerned with attenuation through the troposphere. It is also the region of highest pressure or density and therefore has the highest molecular scatter.

C. GAS COMPOSITION

The atmospheric absorption window regions are defined by molecular absorption, primarily by water vapor and carbon dioxide molecules present in the air. Table 1 lists the main types and concentration of atmospheric gases up to 100 km altitude. Nitrogen and oxygen are by far the most abundant but N₂ and O₂ do not have electric dipole moments and therefore the interaction with EM

radiation is small. Some of the most important molecules impacting propagation have a variable concentration, and these include H₂O, CO₂, and O₃. Water vapor exists primarily in the troposphere and is highly variable from day to day, from season to season, with altitude, and for different geographical locations. Carbon dioxide varies seasonally with a maximum during the early spring and a minimum during the late summer to early fall, and is uniformly mixed with altitude up to 80 km. The variable nature of these important atmospheric gases makes the prediction of atmospheric propagation difficult. The concentration of water vapor also influences particle scattering.

Permanent Gases		Variable Gases	
Gas	Volume Ratio (%) in Dry Air	Gas (and Particles)	Volume Ratio (%)
Nitrogen, N ₂	78.08	Water Vapor, H ₂ O	0 to 2
Oxygen, O ₂	20.95	Carbon dioxide, CO ₂	0.035
Argon, Ar	0.93	Ozone, O ₃	0 to 0.3 ppm*
Neon, Ne	0.0018	Carbon monoxide, CO	0.19 ppm ⁺
Helium, He	5.25 x 10 ⁻⁴	Nitric acid vapor, HNO ₃	(0 to 10) x 10 ⁻³ ppm
Xenon, Xe	8.7 x 10 ⁻⁶	Hydrogen sulfide, H ₂ S	(2 to 20) x 10 ⁻³ ppm
Hydrogen, H ₂	5 x 10 ⁻⁵	Sulfur dioxide, SO ₂	(0 to 20) x 10 ⁻³ ppm

Table 1. Gases Present in Standard Amounts in a Dry Atmosphere. (After [Ref. 4])

Figure 2 shows the low-resolution infrared transmittance of the atmosphere and illustrates the dominance of water vapor over the other atmospheric constituents. The other molecules such as CH₄, N₂O, and CO have

pronounced localized spectral features in the atmosphere even though they have very minor concentrations.

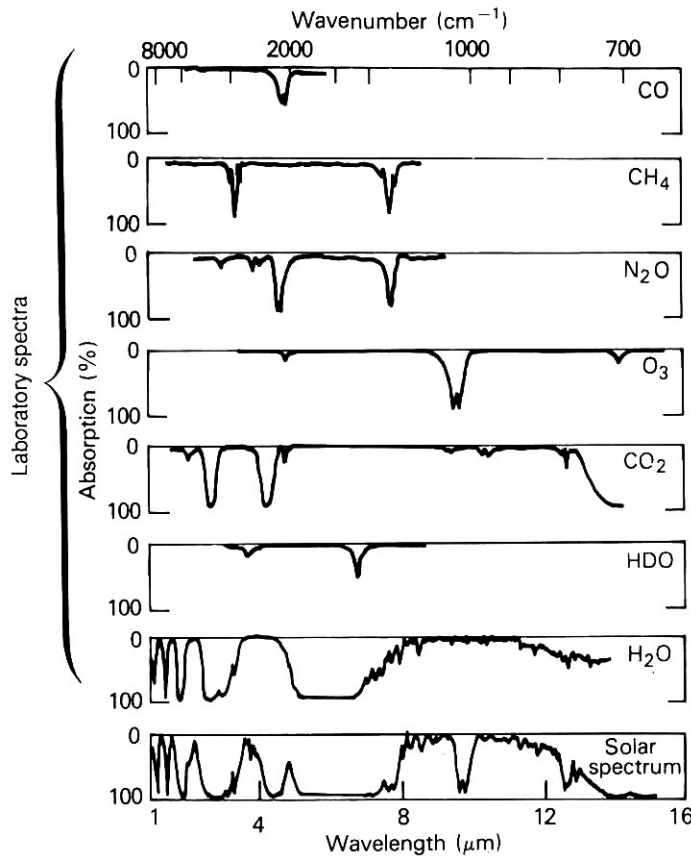


Figure 2. Low-resolution solar spectrum compared with laboratory spectra of atmospheric gases. (From [Ref. 5]).

D. PARTICLE COMPOSITION

Particles vary not only in chemical composition but also in size (from about 0.01 to 10 μm) and shape (spheres, ellipsoids, rods, etc.). Therefore, the description of atmospheric particles is far more difficult than the description of atmospheric molecules. Two basic classes of particles determine the majority of scattering attenuation in the atmosphere: aerosols and hydrometers.

The first class of particles has radii of less than 1 μm . Because these particles are very small, they are suspended in the atmosphere. This mixture is called an aerosol. Scattering by aerosols greatly increases optical attenuation over molecular scattering and is called haze. The particles have the highest concentration levels near the surface of the earth and therefore the highest levels of haze are also near the surface of the earth. Examples are smog, smoke, fine soil particles, cosmic dust, clouds, fog, etc.

The second class of particles, called hydrometers, consists of water-dominated particles in the liquid or solid state. Examples are many types of clouds, mist, fog, rain, freezing rain, hail, snow, ocean spray, etc. These particles are typically larger than 1 μm radius and exist for shorter periods of time than the aerosols.

E. ATMOSPHERIC EFFECTS

The important atmospheric effects to be dealt with are refraction, absorption and scattering by the molecular constituents of the atmosphere and by the suspended particles in it. In the following section we give a brief discussion of these effects, based on the preceding discussions of the origin of refractive index.

The atmospheric refractive index differs from that of free space due to the interaction of the wave electric field with the constituent molecules of the air. Describing this interaction with a simple electron oscillator model leads to an expression of the Sellmeier form for the complex refractive index:

$$\tilde{n}^2 = 1 + \frac{e^2}{m\epsilon_0} \sum_j \frac{Nf_j}{(\omega_j^2 - \omega^2 + i\gamma_j\omega)} \quad , \quad (1)$$

where the summation is over all the atomic and molecular absorption transitions of all species present. In this expression f_j is the "oscillator strength" of the j th oscillator, ω_j the natural radian frequency, γ_j the damping coefficient of the same

transition, N the molecular number density, and e and m the electron charge and mass.

This complex expression for \tilde{n}^2 leads to values of

$$n(\omega) = 1 + \frac{1}{2} \frac{Ne^2}{m\epsilon_0} \sum_j \frac{(\omega_j^2 - \omega^2) f_j}{(\omega_j^2 - \omega^2)^2 + \gamma_j \omega^2}, \quad (2)$$

$$\kappa(\omega) = \frac{1}{2} \frac{Ne^2}{m\epsilon_0} \sum_j \frac{\gamma_j \omega f_j}{(\omega_j^2 - \omega^2)^2 + \gamma_j \omega^2}, \quad (3)$$

for the real and imaginary parts of the refractive index, $\tilde{n}^2 = n - i\kappa$. The imaginary part is proportional to the extinction coefficient, and represents wave absorption at the resonant frequency, while $n(\omega)$, the real part, represents wave dispersion. [Ref. 6].

While the real part of the complex refractive index is important in non-linear propagation effects, the linear attenuation depends mostly on the imaginary part through the absorption coefficient. In the linear regime, except at very high flux density, the attenuation of monochromatic radiation can be described by Bouguer's or Beer-Lambert's Law,

$$I(z) = I(0) \exp(-\alpha_t z), \quad (4)$$

where α_t is a linear extinction coefficient, and z a distance of travel.

The ratio $\frac{I(z)}{I(0)}$ is defined as the transmittance T of the path of length z .

Atmospheric transmittance is a strong function of wavelength, as shown in Figure 1.

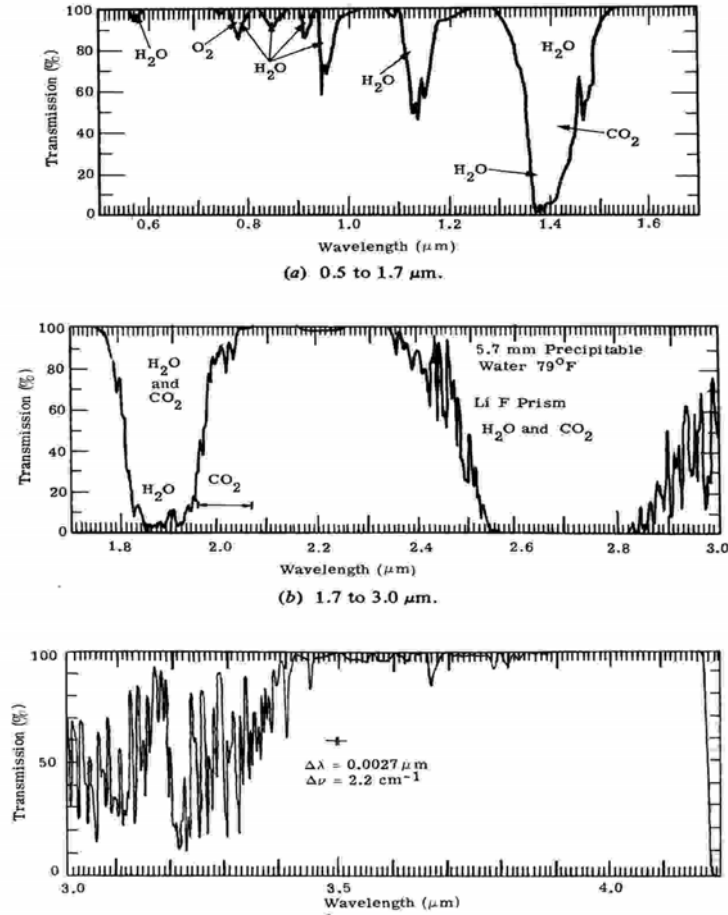


Figure 3. Atmospheric Transmittance as a function of wavelength. (From [Ref. 7]).

It can be seen from Figure 1 that there exist certain "windows" in which EO/IR systems must operate. The extinction shown is caused by a combination of four separate mechanisms which must be considered separately. The total extinction coefficient is the sum of the coefficients for total absorption, α_{abs} , and total non-forward scattering, α_{sca} .

$$\alpha_{total} = \alpha_{abs} + \alpha_{sca} , \quad (5)$$

Both the scattering and absorption coefficients can be divided into components due to the molecules of the air and the aerosol particles suspended in it, i.e.

$$\alpha_{abs} = k_m + k_a , \quad (6)$$

$$\alpha_{sca} = \sigma_m + \sigma_a , \quad (7)$$

where k_m is the molecular absorption coefficient,
 k_a is the aerosol absorption coefficient,
 σ_m is the molecular scattering coefficient,
 σ_a is the aerosol scattering coefficient.

The symbols k and σ used are consistent with the notation used by McClatchey et al. [Ref. 6] in their published tables of data for these quantities.

The relative values of the four coefficients depend strongly on the density and molecular composition of the atmosphere and the composition, number density and size distribution of the aerosols. The order of importance in each of the important atmospheric transmission windows is shown in Table 2.

Atmospheric window	Wavelengths for EO systems	Attenuation coefficients in order of importance
Visible	0.4 μm to 0.7 μm	σ_a, σ_m, k_a
Near Infrared	0.7 μm to 1.2 μm	$\sigma_a, k_a, \sigma_m, k_m$
Middle Infrared	3.0 μm to 5.0 μm	$k_m, \sigma_a, k_a, \sigma_m$
Far Infrared	8.0 μm to 12.0 μm	k_m, k_a, σ_a

Table 2. Order of Significance of Attenuation Coefficients. (From [Ref. 6]).

It can be noted from Table 2 that scattering by both molecule and aerosol is of greater importance in the visible, and absorption in the infrared (particularly 8 to 14 μm). It is important to predict the transmittance of the atmosphere as a function of wavelength and weather conditions. This prediction becomes a complex problem of computer modeling. The problem requires a definition of the composition, density and pressure of the atmospheric gases, together with the frequencies, line strengths and line widths of all the spectroscopic transitions of the gas molecules and the aerosol constituents, and the number size and

composition distributions of the particles. The formulation of transmittance assumes that the respective coefficients due to atmospheric absorption and to aerosol effects are additive; to calculate for a given wavelength and atmospheric condition one requires a suitable model atmosphere with a model for the absorption, and a model for the aerosols for calculation of scattering.

F. ABSORPTION SPECTRAL LINE-SHAPE

The energy structure of a molecule is composed of discrete energy levels. At optical frequencies, the quantum nature of molecules is important. For a two-level system, with energy levels of E_0 (lower) and E_1 (higher), a photon with a frequency such that $E_1 - E_0 = hf_o$ (h is Planck's constant, 6.6256×10^{-34} J sec) is absorbed by this system. Thus only those radiation frequencies whose photon energies match the differences between the molecular energy levels can be absorbed and all other frequencies do not interact. Energy is removed from the photon field at precisely the frequency f_o . Thus, a spectral line is observed at f_o because of the absence of energy relative to the incident photon field.

A real spectral line has an integrated amplitude (or strength S_i) and a halfwidth α_i because the energy levels are not single valued, but instead have a distribution of energies caused by the Heisenberg uncertainty principle, collisions from other molecules, electric fields, magnetic fields, and thermal motion. The resulting absorption feature is illustrated in Figure 4. The strength of the i th absorption line is defined as the entire area under the absorption curve, $\beta(\nu)$. Thus,

$$S_i = \int_0^{\infty} \beta_{abs,i}(\nu) d\nu . \quad (8)$$

The profile, or line-shape function, of the transition is defined as $g(\nu, \nu_o; \alpha_i)$, where α_i is the half-width at half maximum and ν_o is the line center wave number

(frequency). Thus, the absorption coefficient of a single line can be broken down into two factors, the line strength and the line-shape profile:

$$\beta_{abs,i}(\nu) = S_i g(\nu, \nu_0; \alpha_i) . \quad (9)$$

The definition of S_i requires the line-shape profile to be normalized as

$$1 = \int_0^{\infty} g(\nu, \nu_0; \alpha_i) d\nu . \quad (10)$$

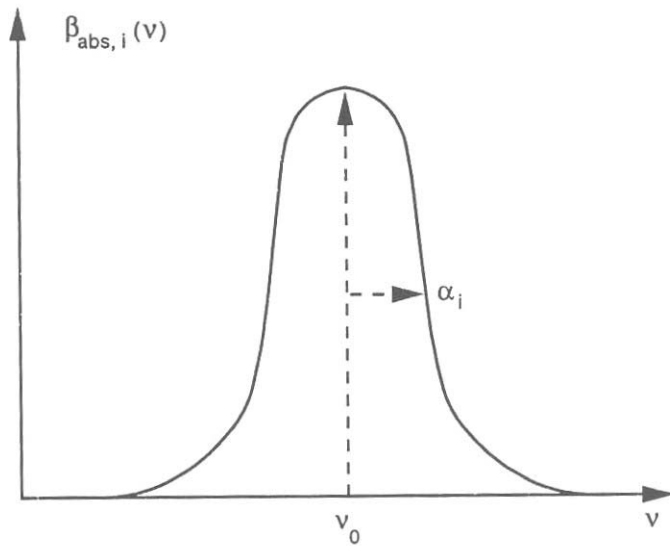


Figure 4. Absorption coefficient of a spectral line, where $\nu_0 = (E_1 - E_0)/hc = f_0/c$, where c is the speed of light. (From [Ref. 4]).

Of course, no molecule has only one spectral line, and a sum over all spectral lines must be made to compute the total absorption as a function of frequency. Therefore,

$$\beta_{abs}(\nu) = \sum_i \beta_{abs,i}(\nu) = \sum_i S_i g(\nu, \nu_i) . \quad (11)$$

G. MOLECULAR ABSORPTION BY ATMOSPHERIC GASES

Absorption by molecules defines the atmospheric windows and is an important mechanism of tropospheric attenuation at millimeter and infrared wavelengths, especially in the marine or relatively humid environments.

Therefore, the understanding and accurate modeling of absorption by atmospheric molecules are important to long-path laser propagation.

As mentioned in the earlier section, absorption of radiation by a molecule is a quantum process and the molecule must undergo a transition from one discrete fixed internal energy state (E_0) to another (E_1). The transition must satisfy the condition

$$\frac{hc}{\lambda} = E_1 - E_0 \quad . \quad (12)$$

Although the levels drawn on energy level diagrams look infinitely narrow, the radiation emitted (or absorbed) in a transition will have a finite bandwidth. The absorption or emission strength of a transition normally has a frequency dependence typical of a classical resonance phenomenon; this is describable by means of a Gaussian or a Lorentzian curve as shown in Figure 5.

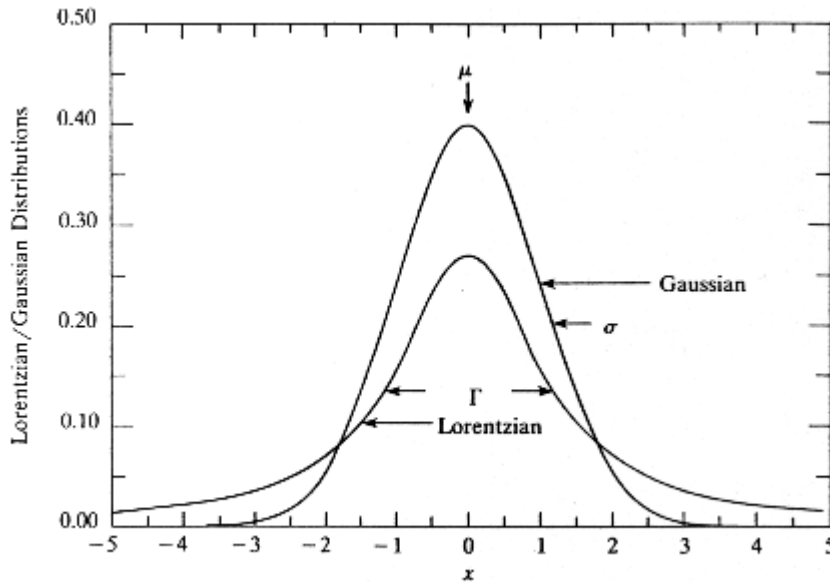


Figure 5. Comparison of normalized Gaussian and Lorentzian curves.

The line-width, r or σ , is usually described as the full width at half maximum of the respective curve. The line-width of an isolated atom or molecule tends to be very small (about 20 MHz or 10^{-4} Angstroms). The line-width may be related to the lifetime of the upper state in the transition by the usual time-bandwidth

product $\Delta\omega\Delta t=1$. In an assembly of atoms or molecules the line-width is modified by the pressure and temperature of the system. As an example, pure carbon dioxide at atmospheric pressure would have a line width of about 5×10^9 Hz.

The imaginary part of the complex refractive index describes absorption. From Equation (3), it can be written as

$$\kappa(\omega) = \frac{1}{2} \frac{Ne^2 f}{m\epsilon_0} \cdot g(\omega), \quad (13)$$

$$\text{where the lineshape function, } g(\omega) = \frac{\gamma}{\omega_0 \left[4(\omega_0 - \omega)^2 + \gamma^2 \right]}, \quad (14)$$

or in terms of frequency,

$$g(\nu) = \frac{\Delta\nu}{16\pi^2\nu_0 \left[(\nu_0 - \nu)^2 + \left(\frac{\Delta\nu}{2} \right)^2 \right]}. \quad (15)$$

The width of the absorption region is γ , the damping factor. For large damping, the absorption curve is broad, for small damping narrow. [Ref. 6].

H. SCATTERING OF RADIATION

Scattering is the process by which the energy in an electromagnetic wave is intercepted and re-radiated into a 4π steradian solid angle. It results from the interaction of the wave field with the electron oscillators in the scattering medium. These are excited by the incoming wave field, behaving as forced harmonic oscillators which re-radiate at the frequency of the incident wave. The secondary wave, however, shows a phase lag from the primary and is dependent on the difference between the wave frequency and the oscillator resonance frequency. Any inhomogeneity in refractive index can cause scattering; in the atmosphere the component gas molecules, aerosol particles of various sizes, fog, rain and hail drops are all effective scatterers. The spatial distribution of the scattered radiation is strongly dependent on the relative magnitudes of the particle size and the wavelength. For particles (of size parameter "a") which are very small

compared with the wavelength ($a \ll \lambda$), the scattering is approximately isotropic; as the ratio of size to wavelength increases, the scattering is concentrated more into the forward hemisphere. For very large scattering objects ($a > \lambda$) forward scattering dominates, and secondary lobes develop at other angles in the radiation pattern. Table 3 shows the size ranges of particles found in the atmosphere.

Type	Radius (μm)	Concentration (cm^{-3})
Air molecules	10^{-4}	10^{19}
Aiken molecules	10^{-3} to 10^{-2}	10^4 to 10^2
Aerosol	10^{-2} to 1	10^3 to 10
Fog droplet	1 to 10	100 to 10
Cloud droplet	1 to 10	300 to 10
Raindrops	10^2 to 10^4	10^{-2} to 10^{-5}

Table 3. Particles responsible for atmospheric scattering. (From [Ref. 4]).

In the small particle regime (up to $a/\lambda \sim 1/10$), the scattering can be described by the relatively simple theory developed by Rayleigh, which predicts scattering proportional to the second power of the volume of the particle and inversely proportional to the fourth power of the wavelength. This describes scattering by atmospheric molecules. For particle sizes greater than about one tenth of the wavelength, the Rayleigh approximation is no longer adequate; the more comprehensive Mie theory (1908) is required. The Mie analysis is used in the FASCODE and LOWTRAN codes to be discussed later, to describe the transmittance due to aerosol particles. For the wavelengths of interest, scattering by the constituent molecular components of the atmosphere can be described by the simpler Rayleigh theory, while the size range of the larger particles gives a size parameter value of order unity.

For the shorter wavelengths, the small particles with the larger number densities dominate the scattering process; for the infrared the secondary peak in the size distribution is of greatest importance. So we see that attenuation by haze is a larger effect at the shorter wavelengths, but the remaining scattering at longer wavelengths (for example 10 micrometers) is dominated by the large particle component, which is very model dependent.

For analytical purposes, it is important to have a good knowledge not only of the size distribution, but also of the chemical composition of the large particle component, since the area scattering efficiency factor depends strongly on refractive index.

I. THERMAL BLOOMING OF HIGH POWER LASER RADIATION

A laser beam propagating through an atmosphere at rest deposits energy into the beam volume through atmospheric absorption. This absorbed energy heats the air, decreasing its density. Decreased density decreases the index of refraction. The relation between density and refractive index is given by the Dale-Gladstone Law [Ref. 8]

$$n = 1 + k(\lambda) \frac{\rho}{\rho_0}, \quad (16)$$

where ρ_0 is the standard density at sea level and $k(\lambda)$ is a function only of λ .

The dependence on the density is essentially linear with a coefficient that is wavelength dependent. The ratio of the air density to the unperturbed air density at standard conditions can be replaced by ratios of the pressures and the temperatures, using the ideal gas law for air of $\rho = P/T$. If one assumes that the increase in pressure in the beam volume relaxes fast enough compared to the laser pulse length, then the pressure in the heated beam volume stays the same

as the ambient pressure and the refractive index change is given by a change in temperature in the beam by the heating which results in a lowering of the density as the pressure drops back to ambient. For wavelengths in the micrometer range the relation between refractive index and temperature in the beam volume is then a simple relation given by

$$n = 1 + k(\lambda) \frac{T_0}{T} . \quad (17)$$

This conversion depends on the thermodynamics of the atmosphere and differs for adiabatic and isothermal cases.

Electromagnetic waves move slightly faster in lower density air. A wave front which is initially a plane wave perpendicular to the beam axis becomes convex in the direction of the propagation. The Gaussian beam intensity profile heats the air near the axis more than does the lower intensity at the edge of the beam. Therefore the density becomes lower on the axis than at the edge. Since the refractive index is dependent on the gas density, a local refractive index gradient develops equivalent to the occurrence of a diverging lens in the beam path, leading to the beam spreading (as depicted in Figure 6.) Due to such spreading of the beam the centerline intensity can decrease rapidly, limiting the irradiance to a value independent of the transmitted power. This self-induced effect is called thermal blooming and is one of the most serious non-linear problems encountered in the propagation of high-energy laser in the atmosphere. The term "non-linear" implies the modification of the propagation medium by the radiation.

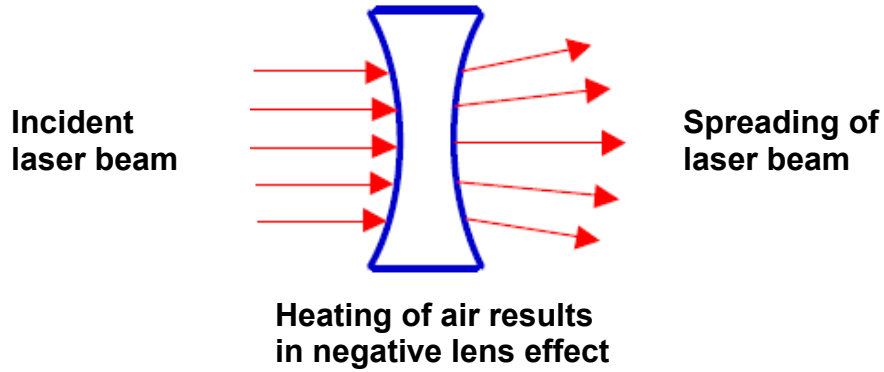


Figure 6. Spreading of laser beam passing through a negative lens.

The exact nature of the thermal blooming effects on the laser beam generally depends on the laser beam characteristics, kinetics of the absorption process, the wind speed, modes of heat transfer and the propagation medium and scenario characteristics. The absorption coefficient of an atmosphere model can therefore be used to make an estimation of the extent of the thermal blooming problem.

III. COMPUTER MODELS FOR ATMOSPHERIC TRANSMISSION

In principle, one could compute the atmospheric extinction by determining the exact composition of the atmosphere over the path of interest and employing the physics of molecular and aerosol extinction. However, because of the wide variations in weather conditions and sparsity of data on some atmospheric constituents, it is desirable to have an engineering approach to atmospheric modeling. To deal with these complex phenomena, the Phillips Laboratory of the Geophysics Directorate at Hanscom Air Force Base, Massachusetts has developed codes to predict transmittance/radiance effects for varying conditions. They have created LOWTRAN (low spectral resolution transmission), FASCODE (fast atmospheric signature code) and MODTRAN (moderate spectral resolution transmission). These codes allow for complex atmospheric transmittance and radiance calculations based on absorption and scattering phenomena for a variety of path geometries. LOWTRAN is a low-resolution (20-cm^{-1}) code, MODTRAN is a moderate resolution (1-cm^{-1}) code, and FASCODE is a high-resolution code. FASCODE uses the HITRAN (high resolution transmission) database directly and LOWTRAN and MODTRAN use the HITRAN database indirectly to determine band-model parameters.

Because of the limitations of the molecular-band model approximation used in LOWTRAN, its accuracy degrades seriously for upper atmospheric regions (above about 40 km). On the other hand, MODTRAN is valid up to 60 km. LOWTRAN is used primarily as an aid for tactical systems operating in the lower atmosphere or on the earth's surface. The model is an excellent predictor at short and medium ranges (up to 20 km) but may be in error at extremely long ranges (~ 100 km). LOWTRAN should not be used for very narrow spectral bandwidth systems such as laser illuminated imaging systems where local line absorption is important. FASCODE is appropriate for applications like laser line calculations.

A. LOWTRAN

LOWTRAN is a FORTRAN computer code designed to calculate atmospheric transmittance and radiance. The code uses a single parameter band model for molecular absorption, which is essentially a curve-fitting match to empirical data. The LOWTRAN model covers the spectral range from 0 to 50,000 cm^{-1} at a low resolution of 20 cm^{-1} . The band model spectral parameters are defined every 5 cm^{-1} . The code was developed in 1971 and is continuously refined, with LOWTRAN 7 being the latest version [Ref. 9]. The atmosphere is represented as 32 layers from 0 to 100 km altitude. 99.99997% of the molecular and particulate atmospheric constituents are found below 100 km. Each layer is horizontally homogeneous. Layer thickness varies from 1 km up to 25 km, 5 km from 25 to 50 km (the top of the stratosphere), and the last two layers are 20 and 30 km thick, respectively. Detailed structure just above the land or sea is not represented by this model and thus model predictions can be inaccurate if nonstandard conditions exist. Attenuation and refractive effects are calculated for each layer and summed along the path. The atmosphere is assumed to be in thermal equilibrium and stable with no inversions.

The major advantage of LOWTRAN is its fast computational capability, which makes it suitable for operational use. The code contains representative (geographical and seasonal) atmospheric models and aerosol models (see Table 4). The aerosol concentration is specified by a meteorological visibility range input. In addition, the user can input radiosonde data as an environmental model or user-defined aerosol model. For any given slant path geometry, it runs in two modes: (1) compute only transmittance and (2) compute both transmittance and radiance. The model can provide radiance and transmittance with and without solar or lunar scattering. LOWTRAN predicts the atmospheric transmittance in homogeneous environments. It is difficult to do predictions at very low altitudes

where the atmosphere changes dramatically, for example, in the first 3 meters above the sea surface, whereby the water vapor content can change significantly leading to a transmittance that is very height dependent. [Ref. 10].

The rural, urban, and maritime models are boundary layer models that apply to the first two kilometers of atmosphere. The troposphere model applies in the troposphere above the boundary layer but can also be used in the boundary layer under extremely good visibility conditions. The Navy Aerosol Model is an empirical model describing the size of aerosol particles close to the surface of the open ocean. The model depends on four parameters; the dimensionless air mass parameter, the average wind speed during the previous 24 hours, the current wind speed and relative humidity. These parameters completely specify the particle size distribution in the model. [Ref. 11].

Environment Models	Aerosol Models
Tropical	Rural
Mid-latitude summer	Maritime
Mid-latitude winter	Urban
Sub-arctic summer	Desert
Sub-arctic winter	Troposphere
1962 Standard	Navy Aerosol Model

Table 4. Atmospheric and aerosol models for LOWTRAN. (From [Ref. 9]).

LOWTRAN has been validated against field measurements and is widely used for many broadband system performance studies [Ref. 12]. However, the single-parameter band model used in LOWTRAN has limited validity with respect to temperature dependence. Calculations above and below room temperature

should be checked against more physically complete codes such as FASCODE. Because of limitations of the molecular band-model approximation used in LOWTRAN, its accuracy degrades seriously for upper atmospheric regions. In particular, LOWTRAN works best at low altitudes with moderate temperatures. High-altitude calculations (> 40 km) will have the least accurate results. Because of the limited resolution of LOWTRAN it should not be applied to laser propagation modeling when local line absorption is important.

B. MODTRAN

MODTRAN is an upgraded version of LOWTRAN that features a two-parameter, band-model code with moderate resolution (1 cm^{-1}) calculations and improved temperature and pressure dependence over LOWTRAN. The main improvements of MODTRAN are:

- a. 1 cm^{-1} resolution band model is used for the latest version MODTRAN 4.0, and thus spectral parameters are calculated every wave number.
- b. A more realistic temperature-dependent model is implemented.
- c. The number of molecules represented is expanded to include water vapor, carbon dioxide, ozone, nitrous oxide, carbon monoxide, methane, oxygen, nitric acid, sulfur dioxide, ammonia, and nitric acid.
- d. High-altitude transmittance/radiance calculations are allowed, up to 60 km. Thus, high-altitude calculations are more valid compared to LOWTRAN calculations.
- e. Replacing an inhomogeneous path with a homogeneous one by using average values for the various band parameters.

MODTRAN has its own spectral database and is appropriate for use in low altitude atmospheric paths (surface to 30 km) and middle atmospheric paths

(between 30 to 60 km). For higher altitude atmospheric paths (above 60 km) band modeling, MODTRAN should be used with caution.

C. HITRAN

HITRAN is the internationally recognized high resolution, line-by-line database for computing the absorption and radiance properties of the terrestrial atmosphere due to molecular transitions. HITRAN archives spectral parameters for 30 molecular species and their significant isotopic variants, covering the electromagnetic spectral range from the millimeter through the visible. In addition, HITRAN contains a supplemental file of cross-sectional data for molecular species that are not amenable to line-by-line formulation. These include species such as chlorofluorocarbons (CFCs) and heavy oxides of nitrogen. HITRAN is used as a direct input to FASCODE and indirect input to the band-modal codes, such as LOWTRAN and MODTRAN. In the latter cases, molecular bands are now run in the line-by-line mode, degraded to the particular resolution of the band model, and then parametrized accordingly. The HITRAN 1998 database was used in this thesis.

D. FASCODE

For studies involving the propagation of very narrow optical bandwidth radiation, for example, lasers, the high resolution afforded by FASCODE, down to 0.1 cm^{-1} , is required. FASCODE is an accelerated line-by-line code developed to address the long computational run time of HITRAN. FASCODE covers the spectral range from 0 to $50,000 \text{ cm}^{-1}$ and models calculations of the absorption line shapes for individual atmospheric species. Characterization of the aerosol and molecular medium in FASCODE is much the same as that for LOWTRAN. However, it is FASCODE that contains the critically precise calculations of absorption (optical depth) per layer, required for exercising the Beer-Lambert

law. The mathematics necessary to determine the appropriate absorption/emission rests with the conversion of individual spectroscopic parameters related to molecular transitions (rotational, vibrational, and electronic), the magnitude of those transitions being governed by lower state populations and the probability of a transition occurring between paired upper and lower states, plus the statistically appropriate line shape factor. Spectral line data for its line-by-line calculations are contained in the HITRAN database. FASCODE attempts to solve for layer optical depth exactly, that is, to better than 1%. Total transmittance is the product of the layer molecular transmittances, with the additional product terms of transmittance effects due to scattering (by both molecules (Rayleigh) and aerosols (e.g. Mie)) and appropriate continua, these being either layer or full path quantities [Ref. 13]. It is in this sense that FASCODE is a physically exact code and achieves a much higher level of accuracy compared to LOWTRAN or MODTRAN. However, due to the complex line-by-line calculations, FASCODE takes a longer time to run compared to the other two codes.

IV. SIMULATION ANALYSIS

A. INTRODUCTION

The computer simulation runs of atmospheric transmission were done using MODTRAN 4.0 and FASCODE 3. The MODTRAN and FASCODE programs use FORTRAN computer language and the data run results were presented in an old output format of an 80-column punch card structure that was used widely in the 1970s. The USAF PLEXUS Release 3, Version 2 (Aug 03) was the user interface program to run MODTRAN and FASCODE. Since PLEXUS is export limited, the PLEXUS runs were performed by Prof Walters and the standard MODTRAN and FASCODE output files were processed by the author. Programs in MATLAB language were written to read and plot the computational run results for analysis.

Three geographical regions were chosen for the study on the atmospheric transmission of a short laser pulse; Korea, Taiwan and Persian Gulf. Initial simulation runs were done on MODTRAN. Effects on the atmospheric extinction of the laser energy were examined by varying the path length and visibility conditions, changing the pulse width of the laser, and comparing different seasons. Differences in the transmission spectrum of the three regions were also compared.

With the results obtained from the MODTRAN runs, five possible windows in the transmission spectrum between 1 to 4 μm were chosen for closer analysis. FASCODE runs based on meteorological data for Korea were conducted. Aerosol effects on atmospheric extinction were eliminated by first examining the input file parameters and calculating the scattering coefficient function, and using this coefficient to calculate and extrapolate a modified transmission spectrum that

includes absorption effects only. Analysis of the absorption coefficient spectrum was done to minimize the effects from thermal blooming of the laser for the chosen wavelength bands.

B. EFFECTS OF THE LASER PULSE WIDTH ON THE TRANSMISSION SPECTRUM

The FEL weapon operating principle is to transmit a pulsed beam of laser energy towards the intended target. The spectral characteristics of the transmitted pulse in the frequency domain is the Fourier transform of the pulse waveform in the time domain. The pulse width will determine the spectral coverage of the transmitted pulse. In general, the narrower the pulse width, the wider will be the spectral coverage in the frequency domain and vice versa. A pulsed laser beam transmitted through the atmosphere will cover a wider band of spectral wavelengths as compared to a continuous wave laser. The result is a modified transmission spectrum. Figure 7 shows a sketch of a free electron pulse waveform with width of 1 pico-seconds (ps). In the frequency spectrum, 1 ps corresponds to a frequency of 10^{12} Hz or a spectral width of about 33 cm^{-1} ($1/\lambda = f/c = 3333 \text{ m}^{-1}$). This means that the spectral width of a 1 ps pulse will cover 33 MODTRAN output data points.

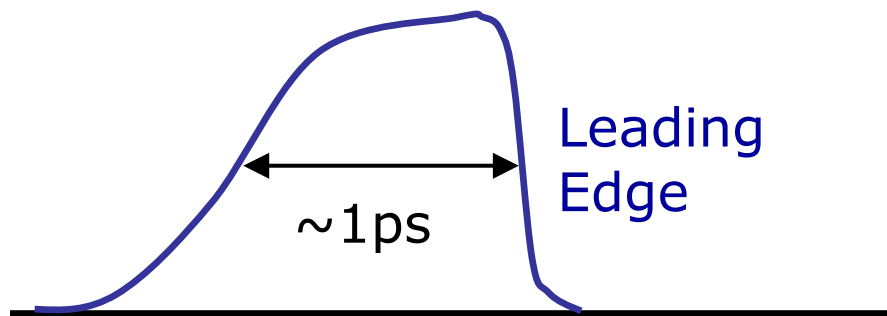


Figure 7. Free Electron Pulse waveform.

To simulate the effect of the laser pulse transmission through the atmosphere, the pulse spectrum was convolved with the transmission spectrum in the frequency domain. A Gaussian function was chosen as an approximate shape to represent the waveform of the FEL pulse. Mathematically, a Gaussian distribution function is expressed as

$$P(t, u, \sigma) = \frac{1}{\sigma\sqrt{2\pi}} \exp\left[-\frac{1}{2}\left(\frac{t-u}{\sigma}\right)^2\right], \quad (18)$$

where u is the mean and σ the standard deviation.

For our purpose of modeling the FEL pulse, 2σ represents the pulse width and the mean is chosen to be zero, and Equation (18) is reduced to a simpler form

$$P(t, \sigma) = \frac{1}{\sigma\sqrt{2\pi}} \exp\left[-\frac{1}{2}\left(\frac{t}{\sigma}\right)^2\right]. \quad (19)$$

Taking the Fourier transform of $P(t, \sigma)$, we get

$$G(f) = \int_{-\infty}^{\infty} e^{-i2\pi ft} \frac{1}{\sigma\sqrt{2\pi}} e^{-\frac{1}{2}\left(\frac{x}{\sigma}\right)^2} dx = Ke^{-2(\pi f\sigma)^2}, \quad (20)$$

where K is a constant.

$G(f)$ is the expression of the Gaussian pulse shape in the frequency domain and is used for convolution with the transmission spectrum. In order to ensure that the values of transmittance for the respective spectral lines are not scaled wrongly as a result of the convolution operation, we need to find a value of K such that $G(f)$ is normalized to a value of one, i.e.,

$$\int_{-\infty}^{\infty} G(f) = \int_{-\infty}^{\infty} Ke^{-2(\pi f\sigma)^2} df = 1. \quad (21)$$

The value of K was found analytically to be $\sigma\sqrt{2\pi}$, and therefore

$$G(f) = \sigma\sqrt{2\pi} e^{-2(\pi f\sigma)^2} . \quad (22)$$

In addition, to ensure an accurate result of the numerical convolution run, the spacing of the points for $G(f)$ must match the 1cm^{-1} spacing of the transmission plot from the MODTRAN runs. For a spectrum of 1 cm^{-1} resolution, df is $3 \times 10^{10}\text{ s}^{-1}$. A plot of $G(f)$ is shown in Figure 8.

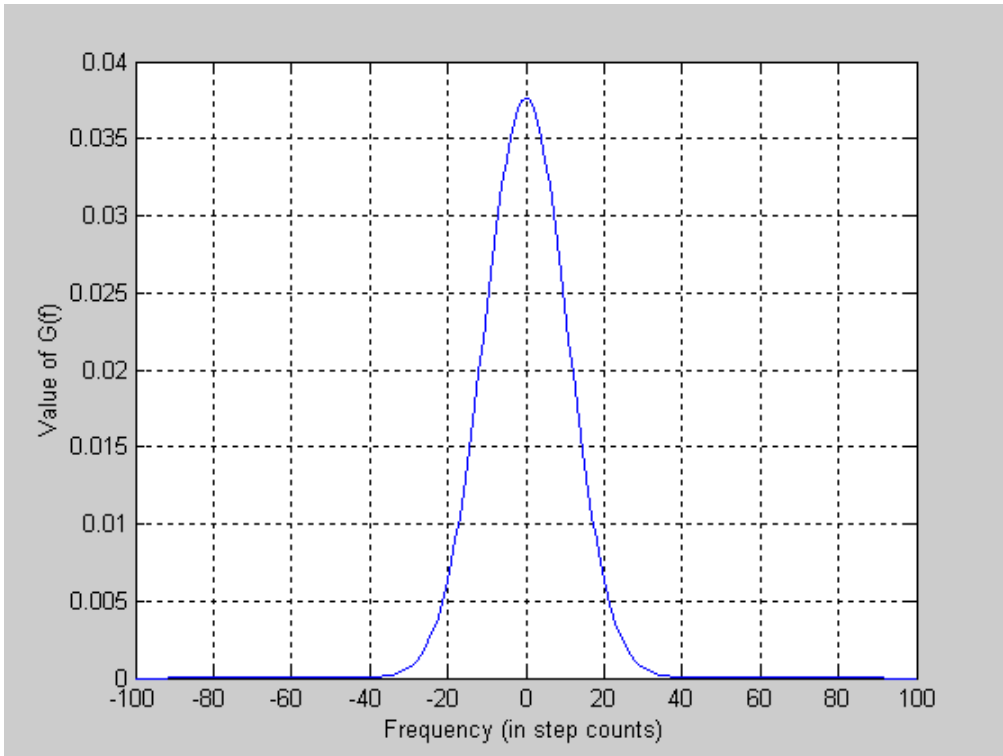


Figure 8. Plot of normalized function $G(f)$.

C. MODTRAN INPUT PARAMETERS

The MODTRAN 4.0 program was used to run the atmospheric transmission data for the following three geographical regions:

- a. Korea, latitude 38°N longitude 129°E
- b. Taiwan, latitude 23°N longitude 120°E
- c. Persian, latitude 29°N longitude 48°E

All runs were done with the Navy Aerosol Model for a maritime clear environment at 10 meters altitude above the selected geographical points, 270 azimuth and horizontal path transmission to simulate the conditions for a ship self defense scenario against an incoming missile attack. Additional input parameters were:

- a. Dates: Jan 1 2004 and July 1 2004.
- b. Time: 0 Zulu for Korea and Taiwan, and 12 Zulu for Persian.
- c. Path length: 2 km and 10 km.
- d. Visibility: 50, 23, 5 and 1 km.
- e. Band: 2400 to 15000 cm^{-1} (or 4.16 to 0.66 μm).

The long wavelength limit of 4 μm was chosen to constrain the optical aperture size and to include the Deuterium Fluoride (DF) laser wavelengths. From optics theory, the spot size (or beam waist) for focusing a Gaussian laser beam at a given distance is proportional to the ratio of wavelength to the diameter of the focusing lens or mirror. [Ref. 14]. Since there is a requirement to keep the beam spot size small to achieve high intensity of energy on the target, operating the laser at longer wavelengths requires a larger optical system.

D. MODTRAN RUN RESULTS

The simulation results for Korea were chosen as a reference for detailed analysis. For standardization of labeling the simulation run plots, the suffix after the geographical region denotes date/path length/visibility. Figure 9 shows the transmission spectrum from MODTRAN data and Figure 10 represents the transmission spectrum for a 1 ps pulse.

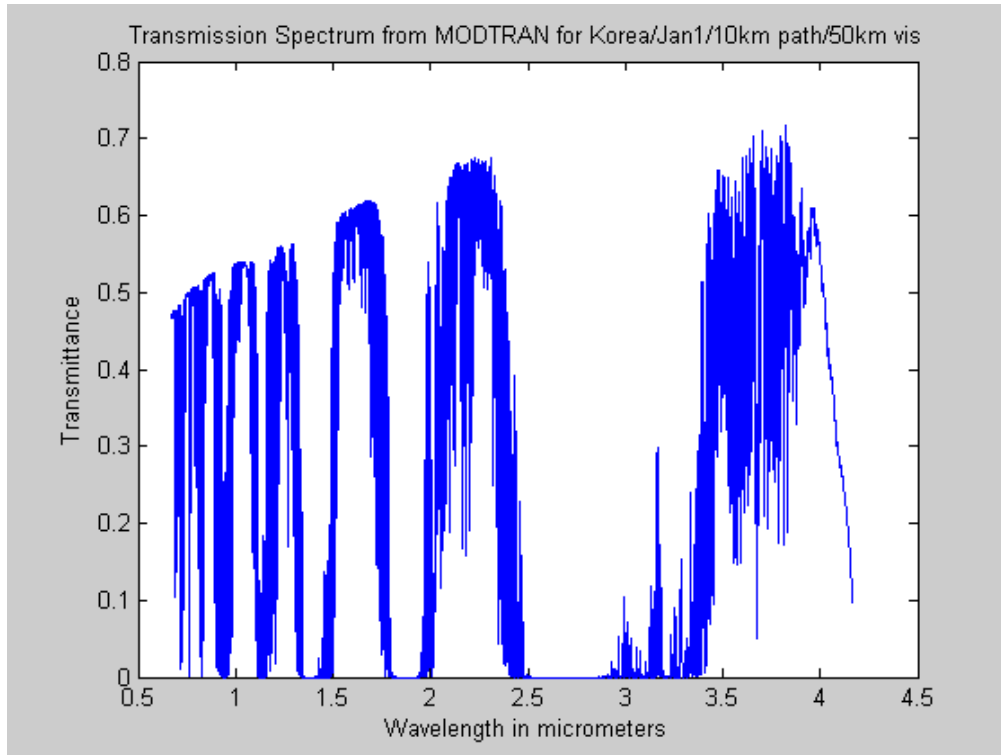


Figure 9. Atmospheric transmission spectrum using MODTRAN for a 10 km long, 10 m high path with 50 km visibility for Korea on 1 Jan.

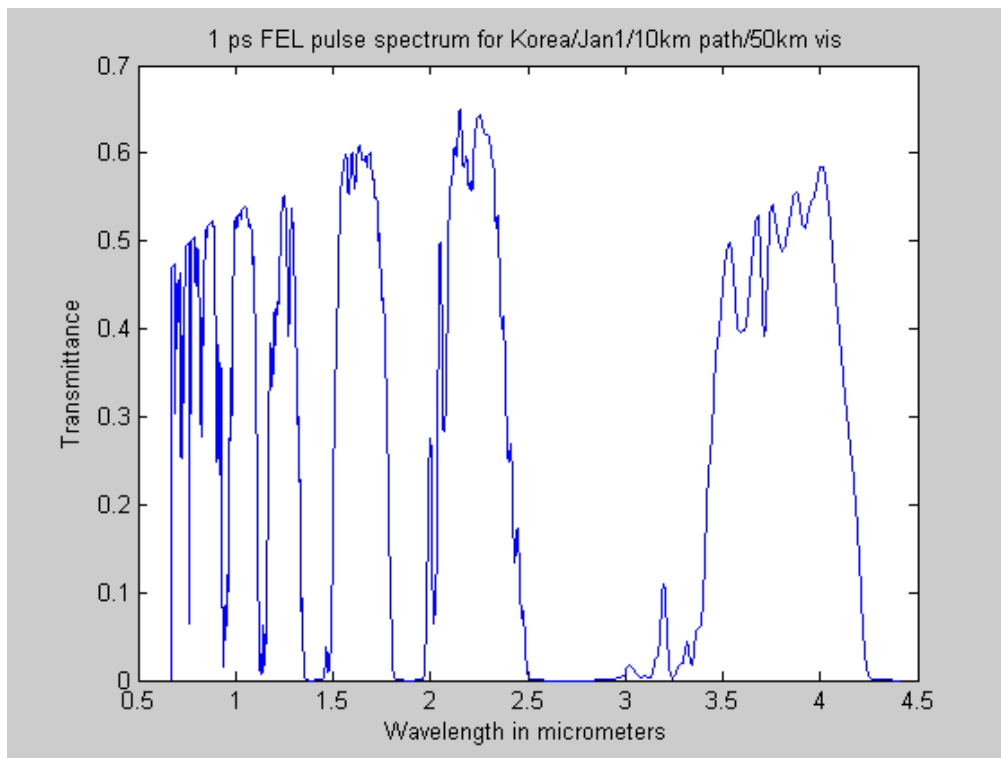


Figure 10. Transmission spectrum for a 1 ps FEL Gaussian pulse using MODTRAN for a 10 km long, 10 m high path with 50 km visibility for Korea on 1 Jan.

Figures 9 and 10 showed that the convolution process produces an averaging of the transmission spectrum. The outlines of the spectra are basically the same for both figures. However, there are some variations in the peak values in transmittance, especially for the 3 to 4 μm band, whereby the FEL pulse spectrum shows lower values.

1. Effects of Different Path Lengths

Figure 11 shows the MODTRAN results for 2km and 10 km transmission paths. As expected, the 10 km path transmission suffers more attenuation compared to the 2 km path. However, the relative amount of attenuation is higher at the shorter wavelengths below 1.5 μm compared to the other bands, because of the aerosol extinction.

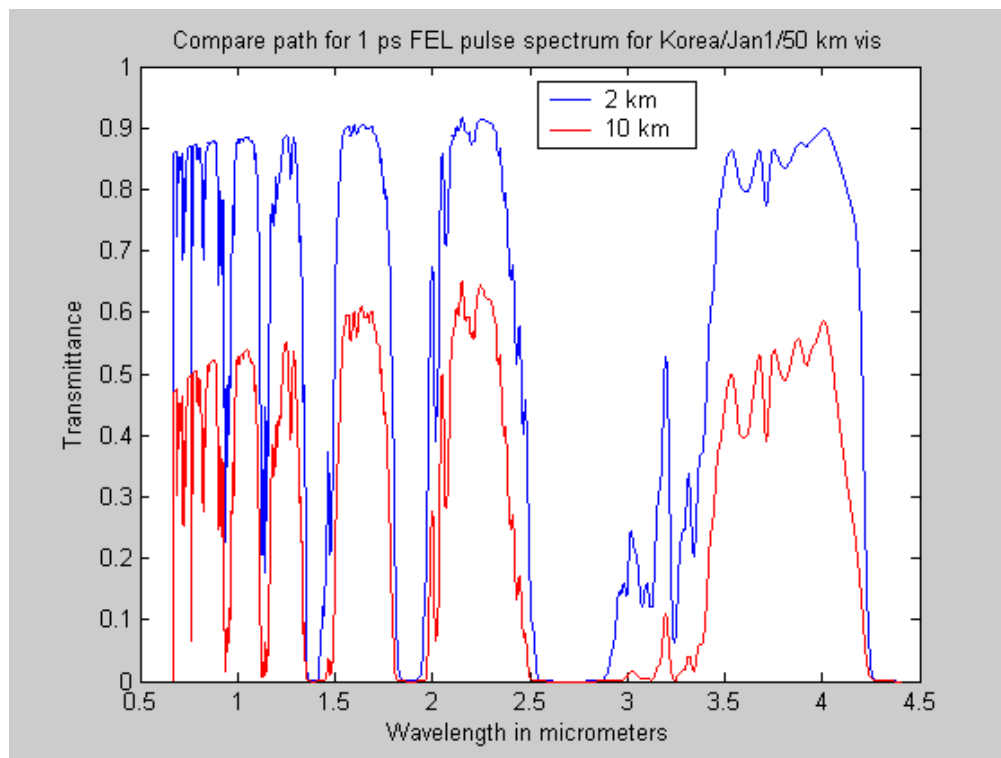


Figure 11. Transmission spectra for a 1 ps FEL Gaussian pulse using MODTRAN for 2 and 10 km long, 10 m high paths with a 50 km visibility for Korea on 1 Jan.

2. Effects of Different Visibility Conditions

Environmental aerosols affect the visibility in the atmosphere. The effect of visibility conditions was examined by running the MODTRAN program for four different visibility values of 50, 23, 5 and 1 km respectively. All runs were based on data for Korea, Jan 1 2004 and 2 km path transmissions. Figure 12 depicts the results of the four spectrum plots. The following observations were made:

- a. Attenuation increases with decreasing visibility conditions.
- b. Amount of extinction varies with wavelength. The higher frequencies are more adversely affected by deteriorating visibility conditions.
- c. At 1 km visibility condition, the transmittance value is less than 5% for all wavelengths.

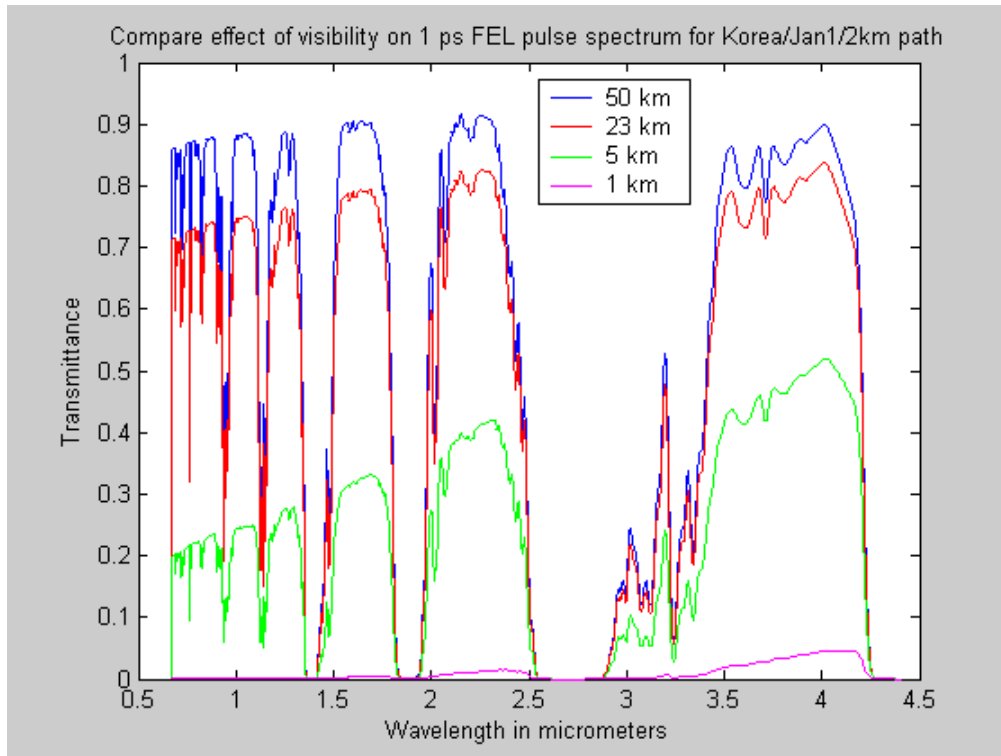


Figure 12. Atmospheric transmission spectra for a 1 ps FEL Gaussian pulse using MODTRAN for 2 km long, 10 m high path with 1, 5, 23 and 50 km visibility for Korea on 1 Jan.

The run results from Figure 12 show that the longer wavelength band of between 3.5 to 4 μm is better for the transmission of laser energy for atmospheric conditions below 5 km visibility.

3. Seasonal Effects

This run was done to compare the transmission spectra for different times of the year. Runs were carried out for Jan 1 2004 and July 1 2004 respectively with the other input parameters remaining the same. Figure 13 shows that at shorter wavelengths, the transmission windows for Korea are not sensitive to the time of year. Only the higher frequencies in the 3.5 to 4 μm window have appreciably lower transmittance values in July compared to January because of higher temperatures and more water moisture content in the air during the summer period.

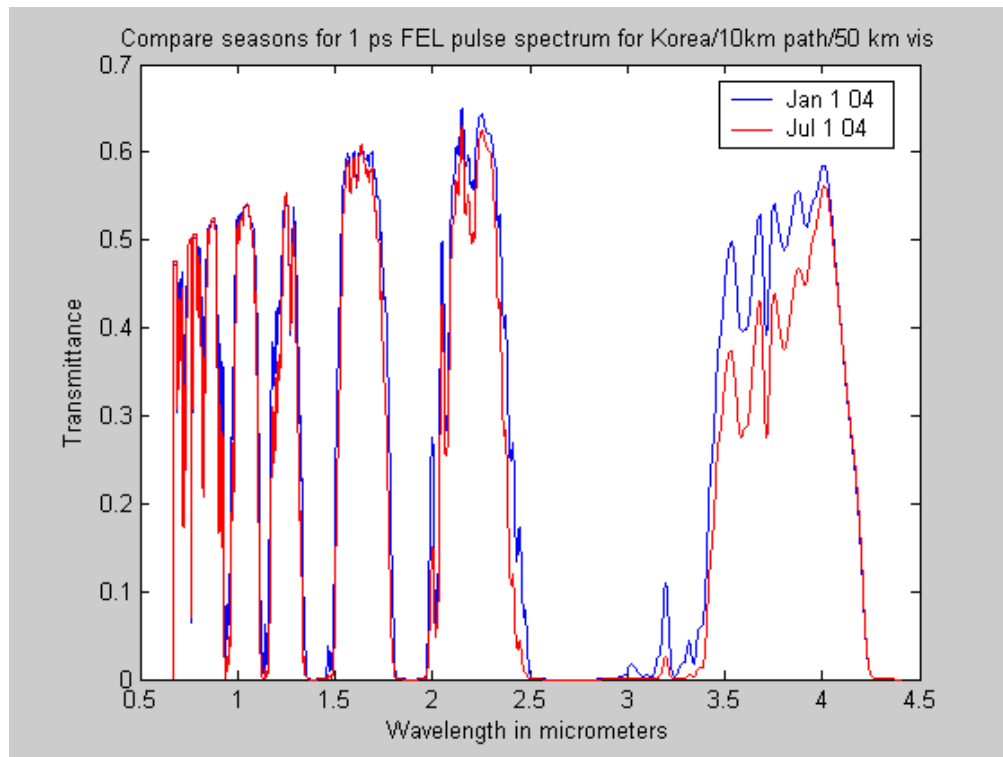


Figure 13. Atmospheric transmission spectra for a 1 ps FEL Gaussian pulse using MODTRAN for a 10 km long, 10 m high path with 50 km visibility for Korea on 1 Jan and 1 July.

4. Effects due to Different Pulse Widths

Figure 14 shows that the spectrum for a 0.25 ps pulse is much smoother and has less detail than the spectrum for the 1 ps pulse. This observation can be explained by the fact that the 0.25 ps pulse has a wider spectral spread in the frequency domain and when it is convolved with the atmospheric transmission spectrum, each point of the spectrum has a resultant value that is averaged over more adjacent data points.

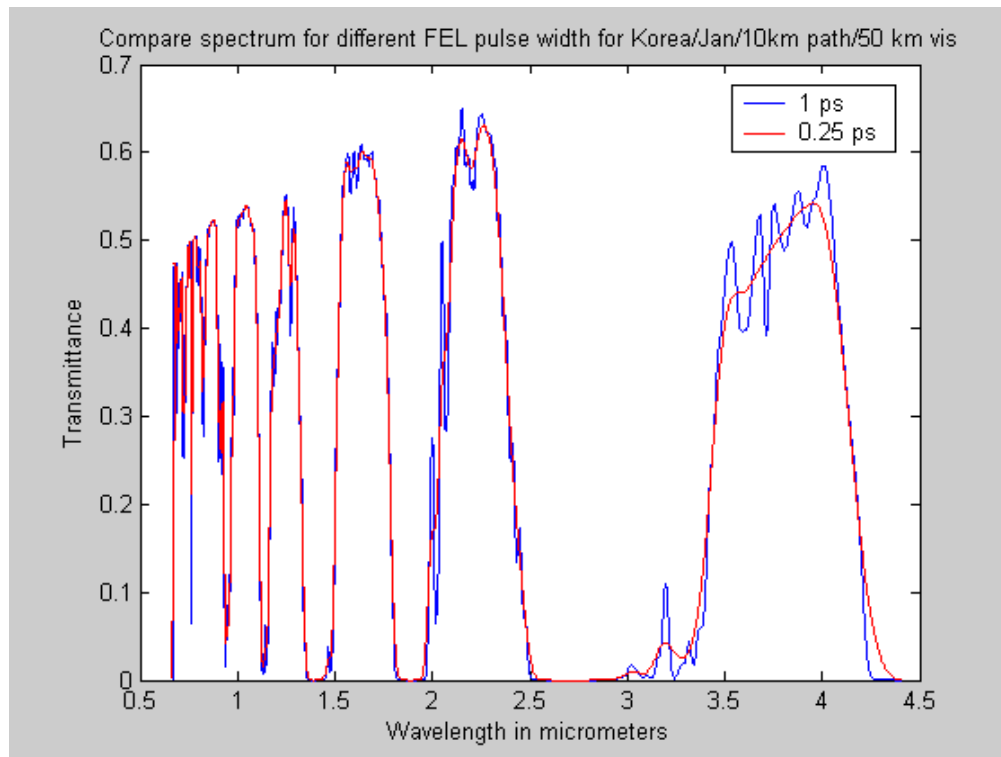


Figure 14. Atmospheric transmission spectra for 0.25 and 1 ps FEL Gaussian pulses using MODTRAN for a 10 km long, 10 m high path for Korea on 1 Jan.

5. Compare Different Regions

The transmission spectra for the three geographical regions of Korea, Taiwan and Persian Gulf appear in Figure 15. The results revealed that there is not much difference in the atmospheric transmittance of EM energy amongst the three regions for the lower wavelengths below 2.5 μm . For the higher wavelengths in the 3 to 4 μm band, the Taiwan area shows more absorption compared to the Persian Gulf or Korea regions. The reason is that the Taiwan

Straits is more humid compared to Korea or Persian Gulf and the absorption by the water vapor molecules are more prominent in the 3 to 4 μm band.

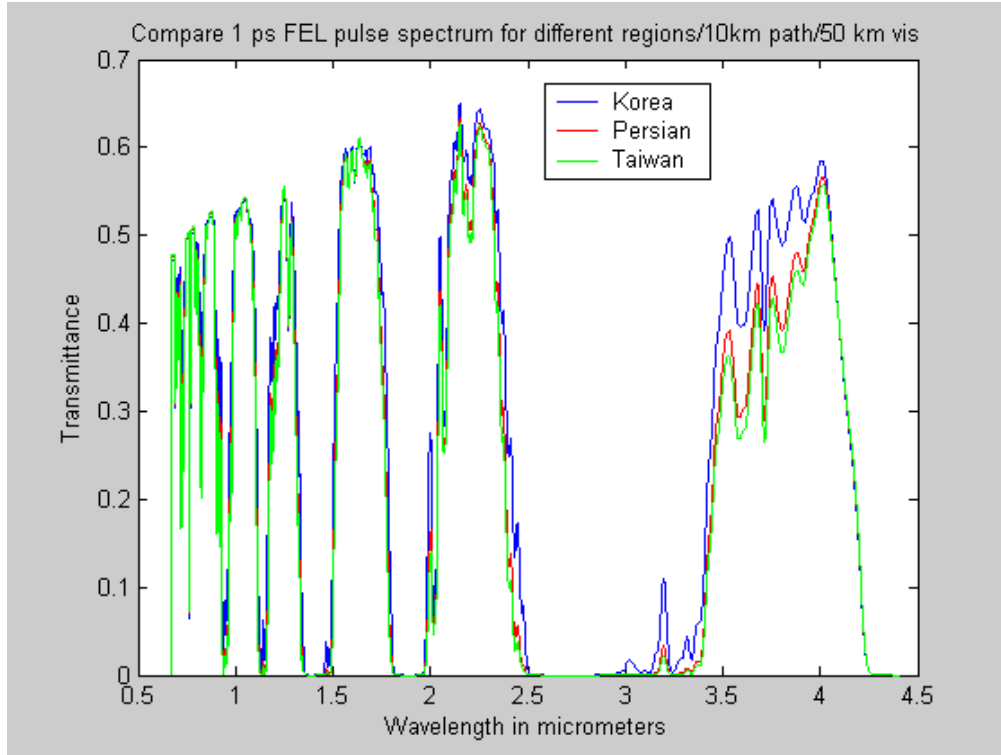


Figure 15. Atmospheric transmission spectra for a 1 ps FEL Gaussian pulse using MODTRAN for a 10 km long, 10 m high path with 50 km visibility for Korea, Persian Gulf and Taiwan on 1 Jan.

E. FASCODE RUN RESULTS

From the MODTRAN run transmission spectra, five windows that provide for good transmission of laser energy through the atmosphere were chosen for further analysis; 0.95 to 1.15 μm (9000 to 10500 cm^{-1}), 1.15 to 1.3 μm (7500 to 9000 cm^{-1}), 1.5 to 1.8 μm (5500 to 6700 cm^{-1}), 2.0 to 2.5 μm (4000 to 5000 cm^{-1}) and 3.8 to 4.2 μm (2400 to 2600 cm^{-1}); as shown in Figure 16. The higher frequency windows below 0.95 μm in wavelength were not considered because

of aerosol extinction associated with poor visibility conditions as evident in Figure 12.

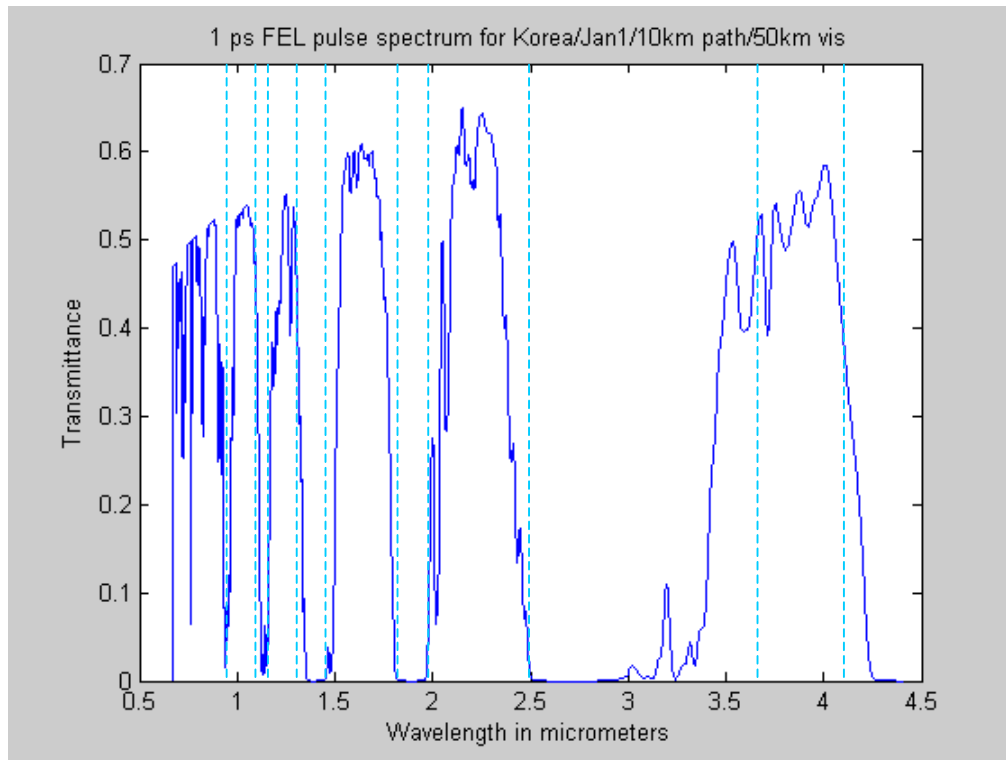


Figure 16. Suitable atmospheric transmission windows for a 1 ps FEL Gaussian pulse.

For the five suitable transmittance windows, finer resolution runs of 0.1 cm^{-1} were conducted using FASCODE for the same three geographical regions and using the Navy Aerosol Model with same values for input parameters as the MODTRAN runs for dates, time of day and altitude. A 10 km horizontal transmission path and 50 km visibility condition were chosen for all runs. The input parameters chosen are meant to represent likely operational scenarios for ship self defense against a cruise missile attack. The main consideration was a 10 m altitude horizontal transmission path. As the FASCODE can only allow a maximum spectral band of 500 cm^{-1} , the following bands were chosen for the runs:

- a. 2400 to 2900 cm^{-1}

- b. 4000 to 4500 cm^{-1}
- d. 4500 to 5000 cm^{-1}
- e. 5500 to 6000 cm^{-1}
- f. 6500 to 7000 cm^{-1}
- g. 7500 to 8000 cm^{-1}
- h. 8000 to 8500 cm^{-1}
- i. 8500 to 9000 cm^{-1}
- j. 9000 to 9500 cm^{-1}
- k. 9500 to 10000 cm^{-1}
- l. 10000 to 10500 cm^{-1}

The output data from the FASCODE runs were concatenated and MATLAB programs were written to plot spectra for the five frequency bands of

- a. 2400 to 2900 cm^{-1} (3.45 to 4.16 μm)
- b. 4000 to 5000 cm^{-1} (2 to 2.5 μm)
- c. 5500 to 7000 cm^{-1} (1.47 to 1.82 μm)
- d. 7500 to 9000 cm^{-1} (1.11 to 1.33 μm)
- e. 9000 to 10500 cm^{-1} (0.95 to 1.11 μm).

F. ABSORPTION COEFFICIENT SPECTRUM

Besides the overall extinction of the laser pulse energy, it is important to assess the extent of thermal blooming. As discussed in Chapter II, thermal blooming is a result of localized heating of air by the laser beam and is proportional to the absorption coefficient. Hence, knowing the absorption coefficient for each spectral frequency will be useful in assessing at which frequency bands thermal blooming is likely to be more severe.

From Equation (4), the transmittance, $T(z)$, as a function of distance is related to the absorption and scattering coefficient by $T(z) = \exp[-(\alpha_{abs} + \alpha_{sca})z]$. Dividing $T(z)$ by $\exp(-z\alpha_{sca})$ gives the absorption component $T(z) = \exp(-z\alpha_{abs})$. From $T_{abs}(z)$ the absorption coefficient is

$$\alpha_{abs} = \frac{-\ln T_{abs}(z)}{z}. \quad (23)$$

The values of $\exp(-z\alpha_{sca})$ can be found in one of the output files for FASCODE runs (under file tape 6). However, because they appear as a constant value over a range interval of 5 cm^{-1} wavenumbers, it is not correct to carry out a direct multiplication of the $\exp(-z\alpha_{sca})$ values to the $T(z)$ data which has an interval of 0.1 cm^{-1} . To interpolate the values of $\exp(-z\alpha_{sca})$ down to each 0.1 cm^{-1} wavenumber, the $\exp(-z\alpha_{sca})$ values were plotted by Microsoft Excel program and a 2nd order polynomial expression was computed to fit the points. By using the 2nd order polynomial line equation, the value of $\exp(-z\alpha_{sca})$ for each 0.1 cm^{-1} wavenumber was calculated by a MATLAB program which also compute and plot α_{abs} against wavelength. Figures 17 to 20 shows the related plots between extinction spectrum, absorption spectrum, absorption coefficient and FEL pulse absorption coefficient plots for the Korea, Jan 1, 2004, 10km runs with 50km visibility for a 1 ps FEL Gaussian pulse.

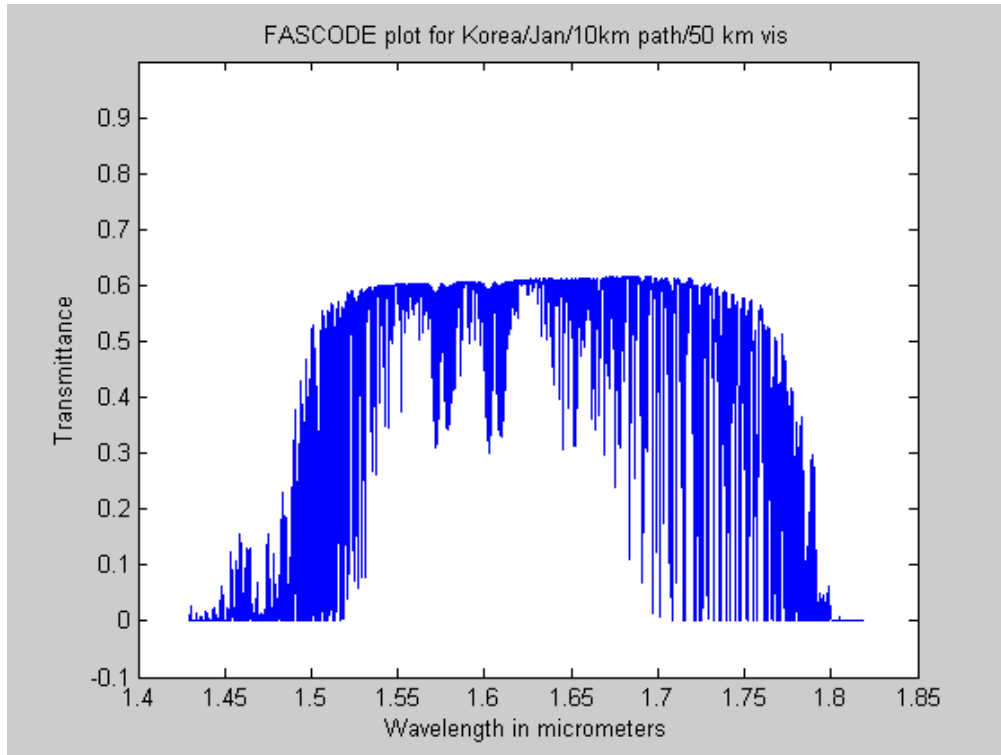


Figure 17. Atmospheric transmission spectrum using FASCODE for a 10 km long, 10 m high path with 50 km visibility for Korea on 1 Jan.

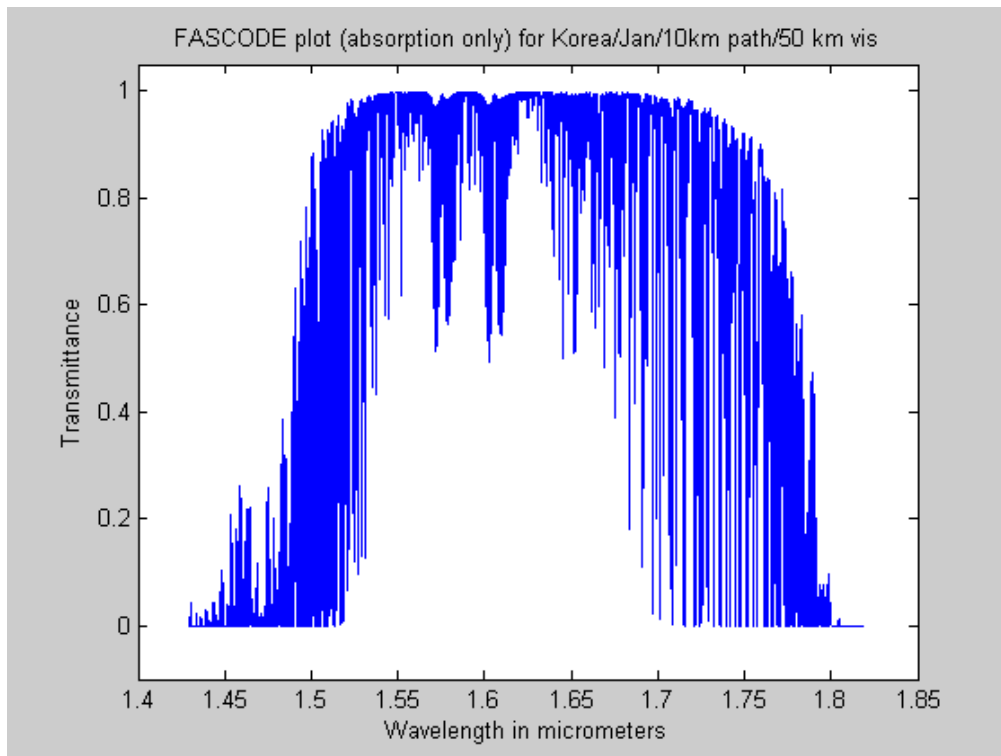


Figure 18. Molecular transmission spectrum using FASCODE for a 10 km long, 10 m high path for Korea on 1 Jan.

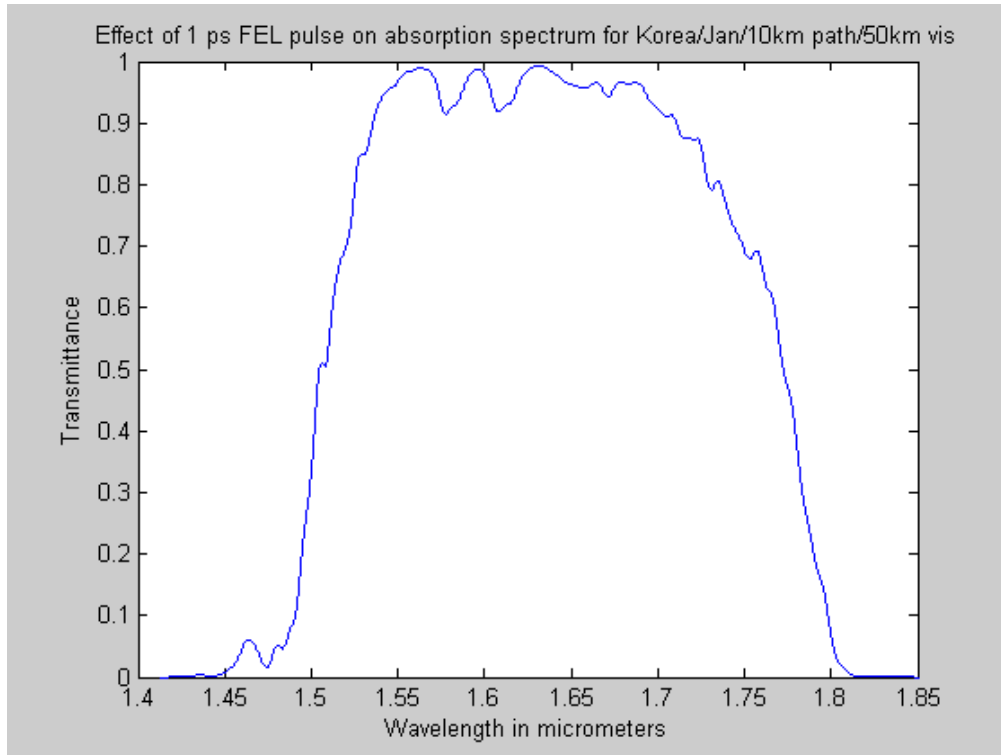


Figure 19. Molecular transmission for a 1 ps FEL Gaussian pulse using FASCODE for a 10 km long, 10 m high path for Korea on 1 Jan.

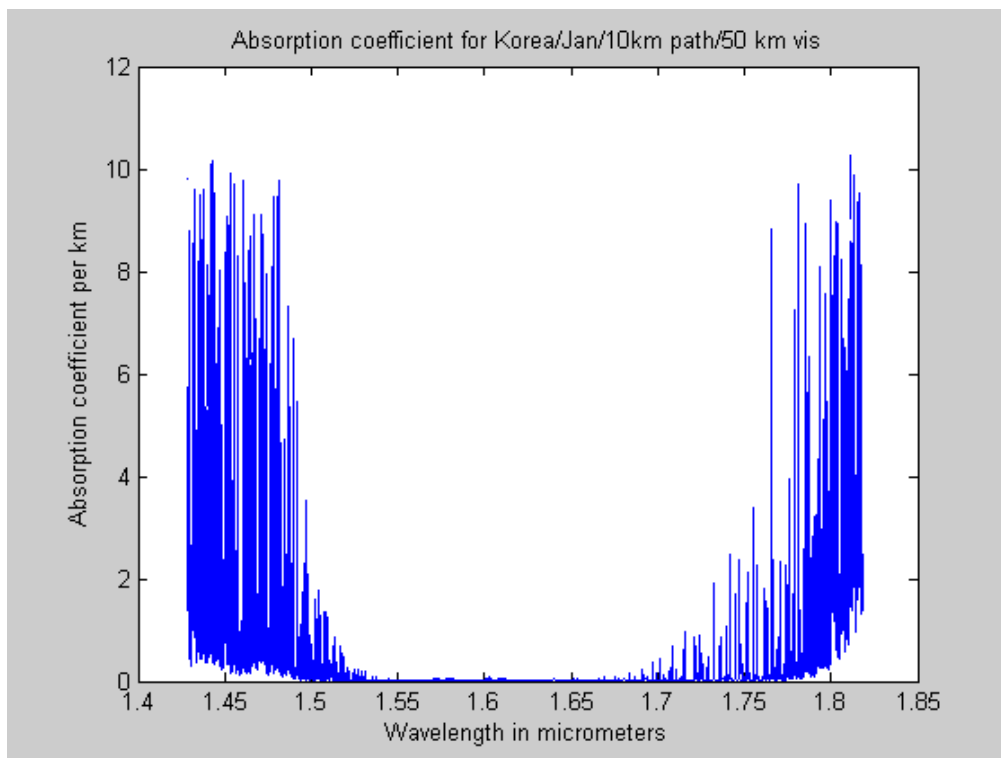


Figure 20. Absorption coefficient using FASCODE for a 10 km long, 10 m high path for Korea on 1 Jan.

Comparing Figures 17 and 18, the absorption spectrum is similar to the extinction spectrum (Figure 17) except that the former has higher transmittance values, with the maximum close to 100% compared to about 60% for the extinction spectrum. Aerosol scattering accounted for about 40% of the energy loss through atmospheric transmission for the chosen test run parameters.

The absorption coefficient lines as plotted in Figure 20 are consistent with the general outline of absorption spectrum in Figure 18 with high coefficient values coinciding with the low transmittance values. By comparing Figures 21 and 22, it is interesting to note that the transmission of the 1 ps FEL pulse reduces the absorption coefficient to about 14% of the peak values. The result suggests that an FEL pulse laser can be less affected by atmospheric absorption than a monochromatic laser, because it can use the regions between absorption lines.

Figures 23 and 24 compare the extinction coefficient and absorption coefficient graphs by magnifying the scales of the plots. The two coefficient plots are the same form except for their relative values. For each corresponding wavenumber, the extinction coefficient value is higher than the absorption coefficient by 0.05 per km for this frequency band. This observation implies that for FASCODE, the correction factor for the scattering effect is fairly linear across this narrow band of frequencies.

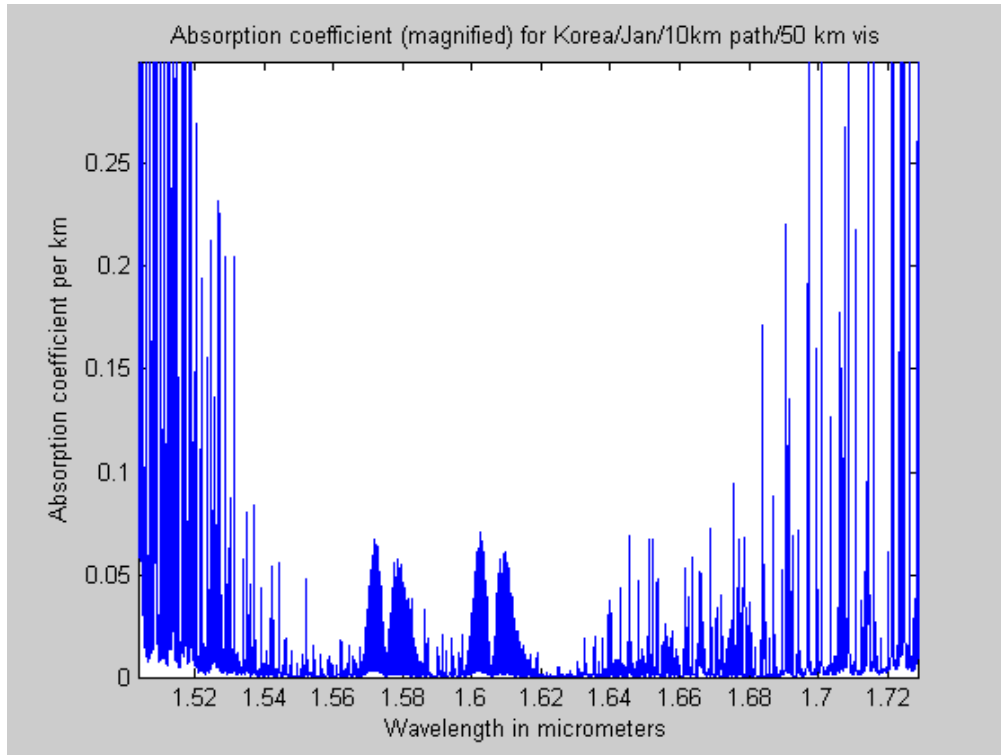


Figure 21. Absorption coefficient from 1.51 to 1.73 μm using FASCODE for a 10 km long, 10 m high path for Korea on 1 Jan.

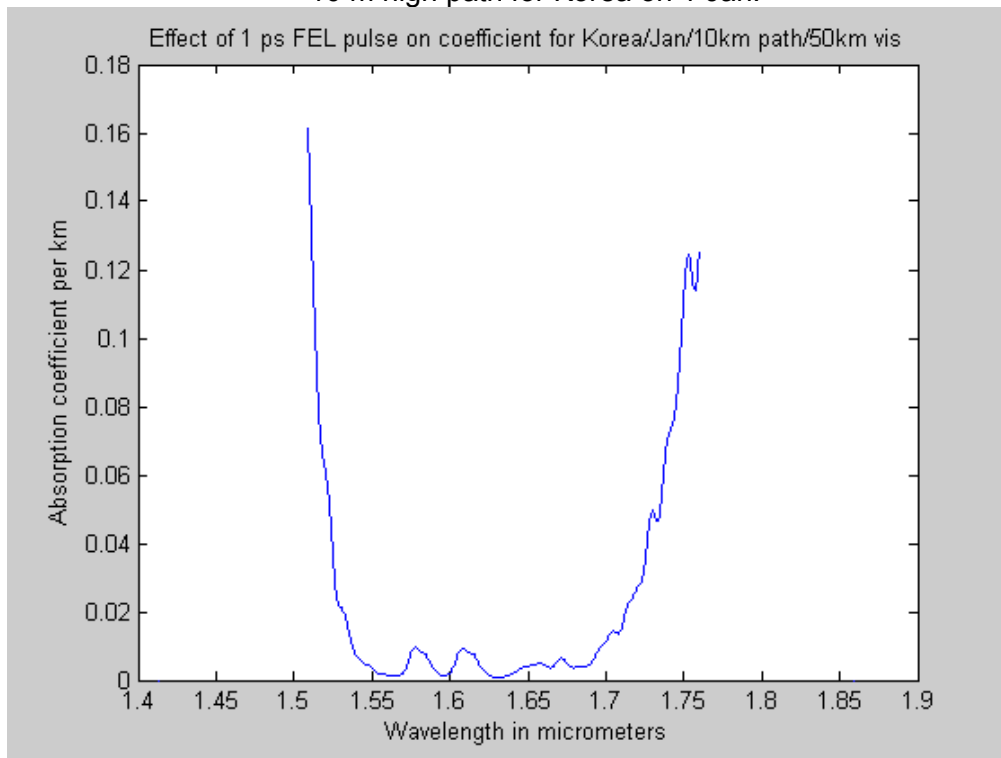


Figure 22. FASCODE absorption coefficients convolved with 1 ps Gaussian pulse for a 10 km long, 10 m high path with 50 km visibility for Korea on 1 Jan.

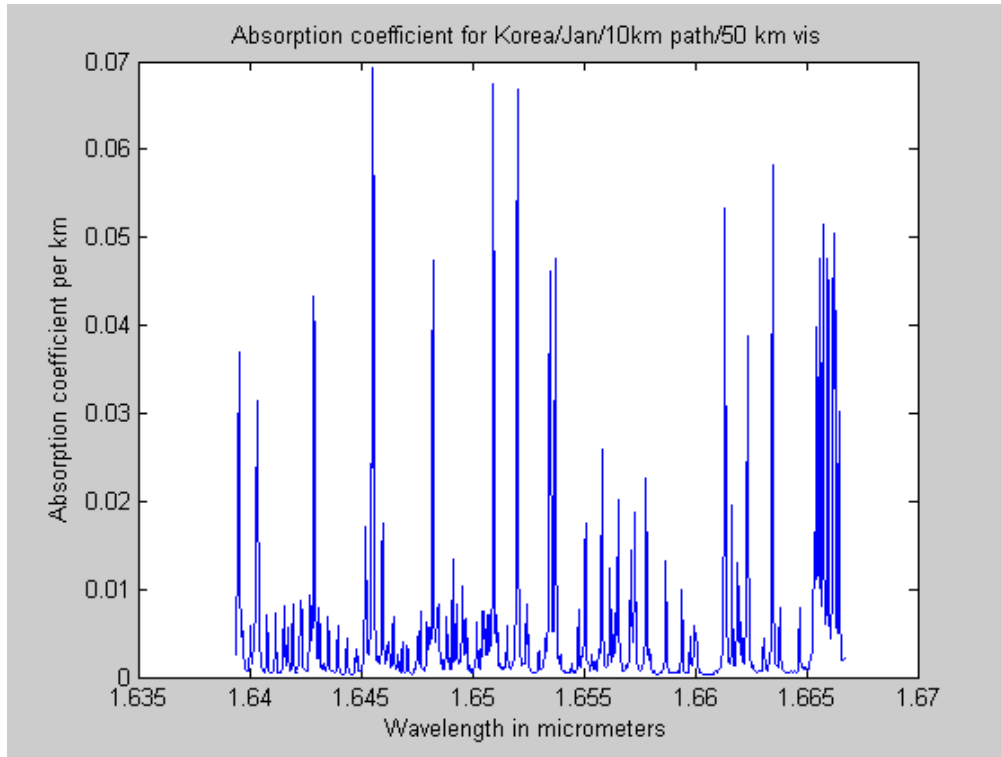


Figure 23. FASCODE absorption coefficients from 1.635 to 1.666 μm for a 10 km long, 10 m high path for Korea on 1 Jan.

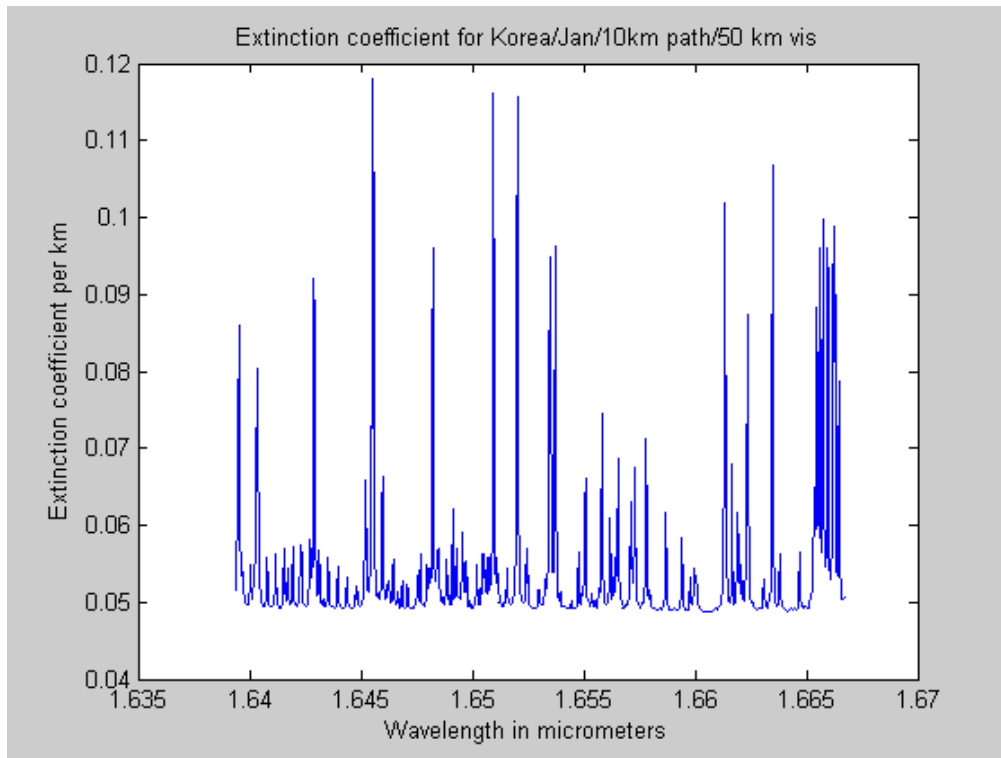


Figure 24. FASCODE extinction coefficient from 1.635 to 1.666 μm for a 10 km long, 10 m high path for Korea on 1 Jan.

1. Absorption Coefficients for Existing High Energy Lasers

Figures 23 to 27 show the absorption coefficient spectrum for known operational gas and chemical laser wavelengths such as the Nd Yag (1.0641 μm), Oxygen Iodine (1.3150 μm) and Deuterium Fluoride (3.8007, 3.8375, 3.8757, 3.9155 and 3.9565 μm).

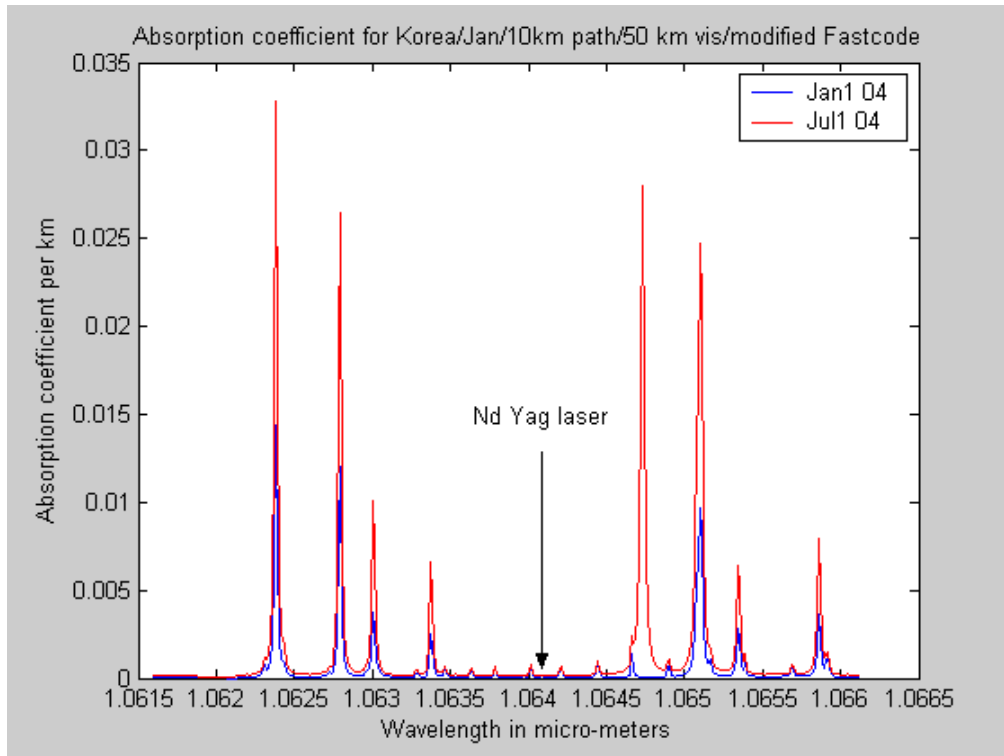


Figure 25. Absorption coefficient near the of Nd Yag laser operating wavelength.

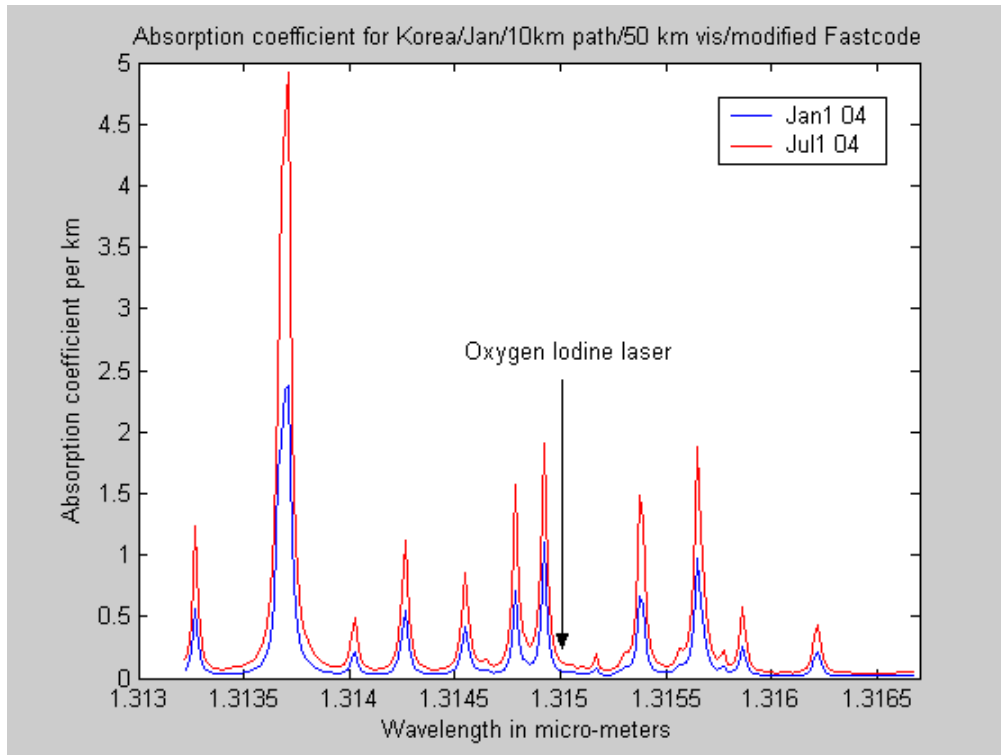


Figure 26. Absorption coefficient near the oxygen-iodine laser operating wavelength.

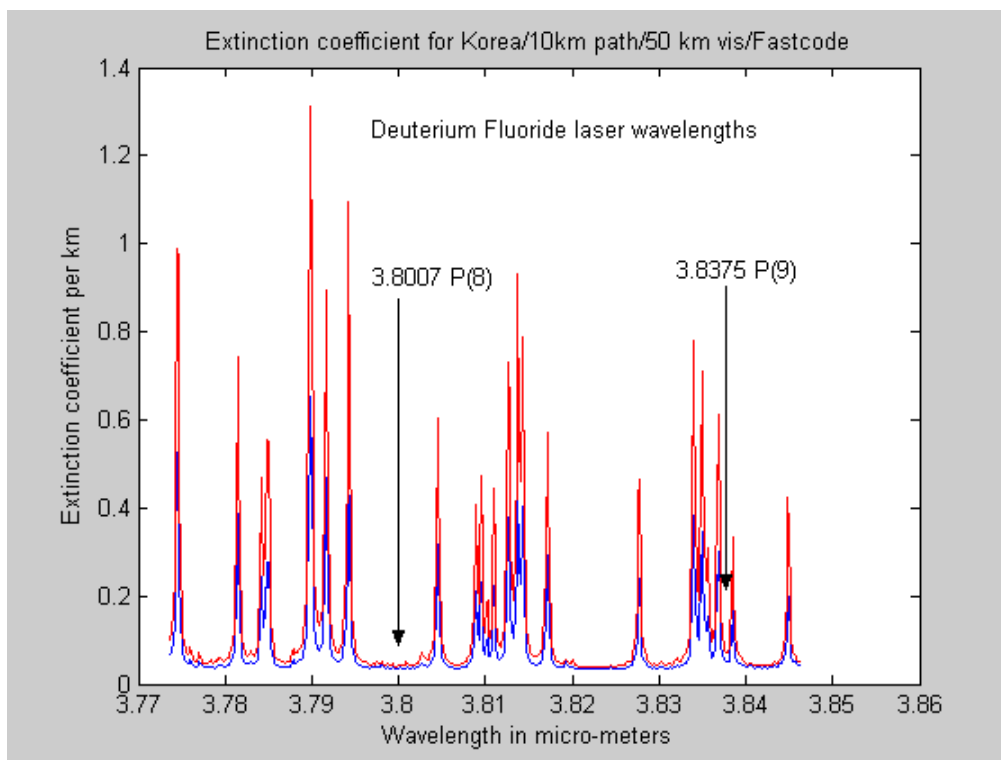


Figure 27. Absorption coefficient near the P(8) and P(9) deuterium fluoride laser operating wavelengths. [Ref. 15].

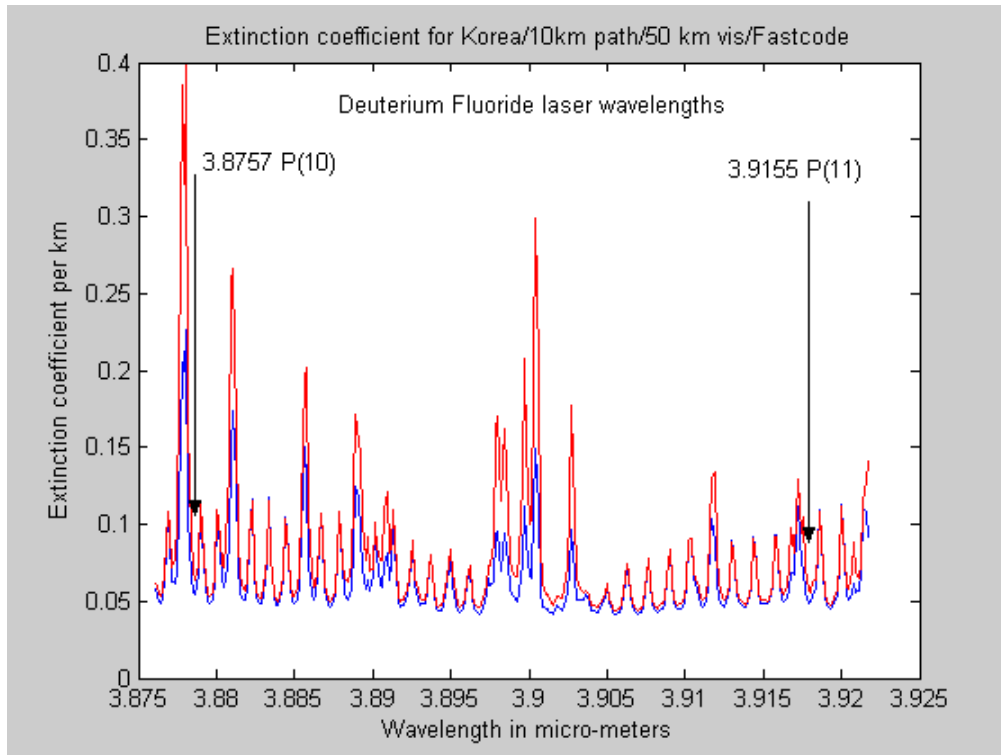


Figure 28. Absorption coefficient near the P(10) and P(11) deuterium fluoride laser operating wavelengths. [Ref. 15].

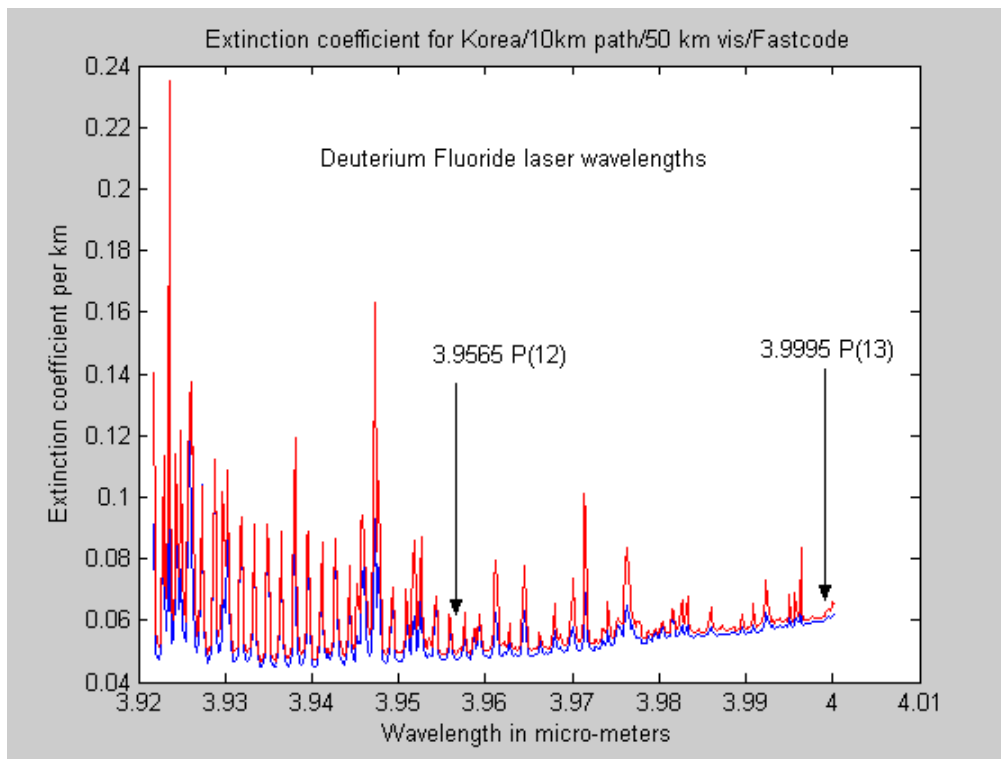


Figure 29. Absorption coefficient near the P(12) and P(13) deuterium fluoride laser operating wavelengths. [Ref. 15].

G. OPTIMAL WAVELENGTH BANDS

It was shown in the earlier sections from the MODTRAN runs that the transmission spectrum varies with path length and visibility conditions. To suggest suitable operating frequencies for the employment of an FEL, the analysis should represent likely operating scenarios. A 2 km engagement range only leaves about 3 seconds for a Mach 2 sea-skimming missile. Therefore, a more realistic transmission path length is 10 km. Korea was chosen as the region for study with both Jan 1, 2004 and July 1, 2004 dates being selected. Lacking realistic visibility conditions for the Korean peninsula, 50 km visibility was used to investigate the atmospheric molecular absorption leaving the atmospheric scattering issue for further study. A 1 ps (2σ) Gaussian pulse was convolved with the 0.1 cm^{-1} FASCODE spectra for the five frequency bands of 0.95 to 1.11 μm , 1.11 to 1.33 μm , 1.47 to 1.82 μm , 2 to 2.5 μm and 3.45 to 4.16 μm . Transmission spectrum and absorption coefficient plots were compared to find the range of suitable wavelengths that give good transmittance and low absorption coefficient values. The molecular absorption spectrum was chosen over the extinction spectrum because we cannot verify the validity of the Navy Aerosol Model results incorporated into the MODTRAN and FASCODE calculations. In addition, the energy scattered out of the beam by aerosols will not contribute to thermal blooming, though aerosol absorption and evaporation of water droplets will contribute. Figures 28 to 37 show the result of the runs for the five selected bands for both Jan 1 and July 1, 2004.

Suitable wavelength windows were selected from either the Jan 1 or July 1, 2004 spectra for the date with a narrower transmittance window by meeting the following two criteria:

- a. Transmittance value of at least 90%, 95% and 99% respectively over a 10 km long, 10 m high horizontal path.
- b. Absorption coefficient value of less than 0.02 per km.

Table 5 summarizes the suitable wavelengths. The first four bands from 0.95 μm to 2.5 μm were able to meet the criteria of at least 90% transmittance and absorption coefficient of not more than 0.02 per km. However, there are no wavelengths in the 3.45 to 4.16 μm band that can meet the two specified criteria. The best wavelength window for this band is chosen for 70% transmission and absorption coefficient less than 0.04 per km.

From Table 5, the optimal wavelength windows for molecular atmospheric absorption are between 1.03 μm and 1.06 μm , and around 1.241 and 1.624 μm . This band provides a transmittance of more than 99%. However, as noted earlier, the main drawback of operating in a lower wavelength band is the strong extinction of energy from aerosol scattering.

Wavelength Bands	Suitable wavelength windows for various values of T(z) in μm			
	T(z) > 90% $\alpha_{\text{abs}} < 0.01/\text{km}$	T(z) > 95% $\alpha_{\text{abs}} < 0.005/\text{km}$	T(z) > 99% $\alpha_{\text{abs}} < 0.001/\text{km}$	* T(z) > 70%
0.95 to 1.11 μm	0.990 -1.075	0.992 - 0.998 1.002 -1.006 1.01 - 1.067	1.030 -1.060	N.A.
1.11 to 1.33 μm	1.230 -1.260 1.271 -1.283	1.235 -1.256	1.241	N.A.
1.47 to 1.82 μm	1.530 -1.680	1.535 -1.565 1.58 -1.595 1.610 -1.660	1.624	N.A.
2 to 2.5 μm	2.125 -2.140 2.220 -2.245	N.A	N.A	N.A.
3.45 to 4.16 μm	N.A	N.A	N.A	3.91 - 3.94

Table 5. Summary of suitable wavelength bands for FEL operation for a 10 km horizontal path, 10 m above the ocean with no aerosol extinction.

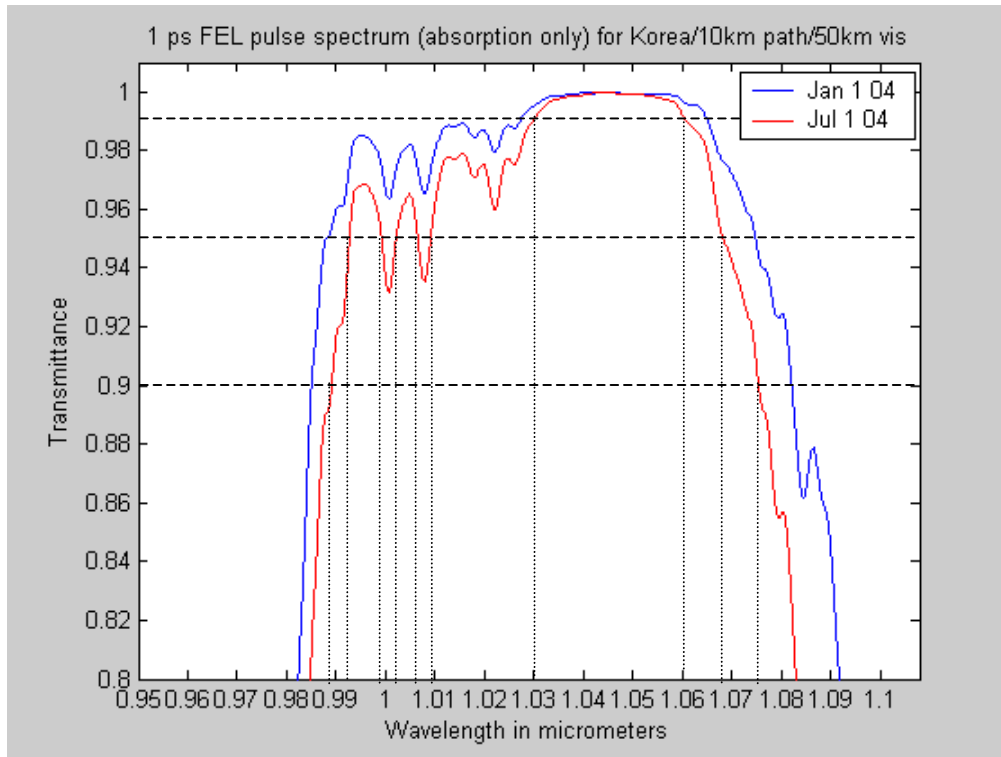


Figure 30. Molecular transmission for a 1 ps FEL Gaussian pulse from 0.95 to 1.11 μm using FASCODE for a 10 km long, 10 m high path for Korea on 1 Jan and 1 July.

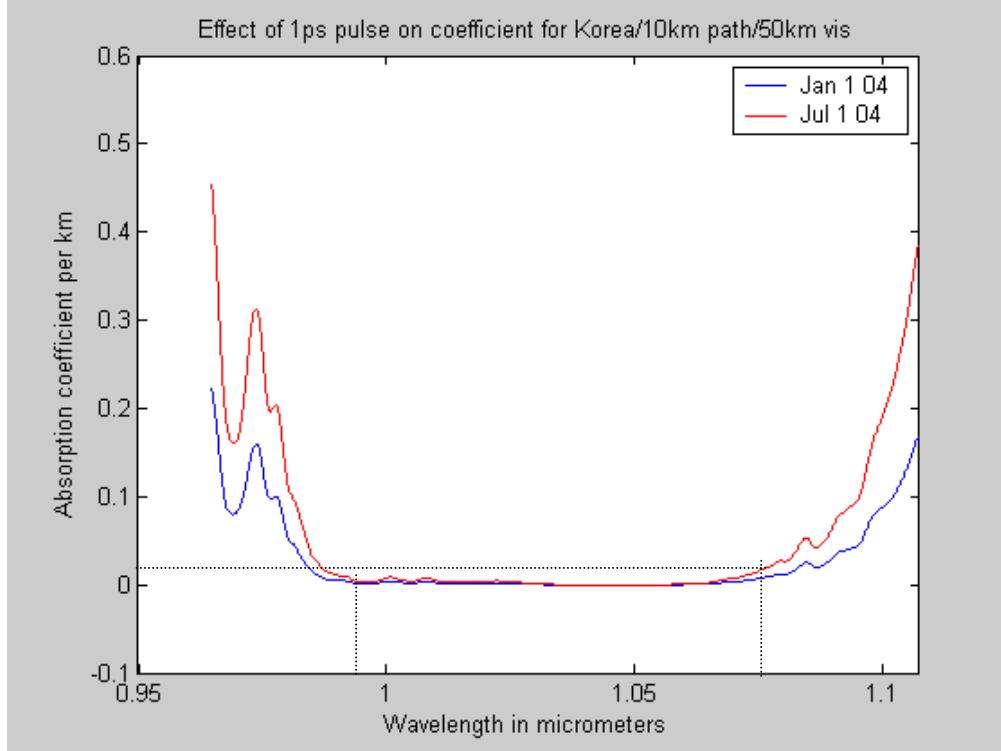


Figure 31. Absorption coefficient for a 1 ps FEL Gaussian pulse from 0.95 to 1.11 μm using FASCODE for a 10 km long, 10 m high path for Korea on 1 Jan and 1 July.

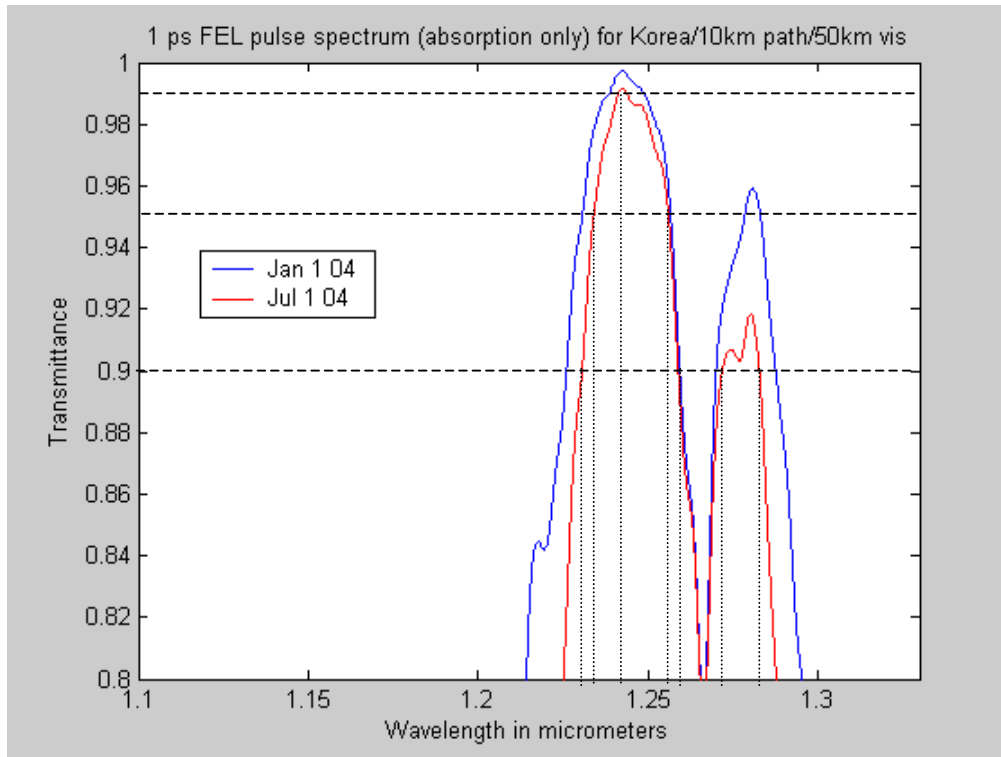


Figure 32. Molecular transmission for a 1 ps FEL Gaussian pulse from 1.11 to 1.33 μm using FASCODE for a 10 km long, 10 m high path for Korea on 1 Jan and 1 July.

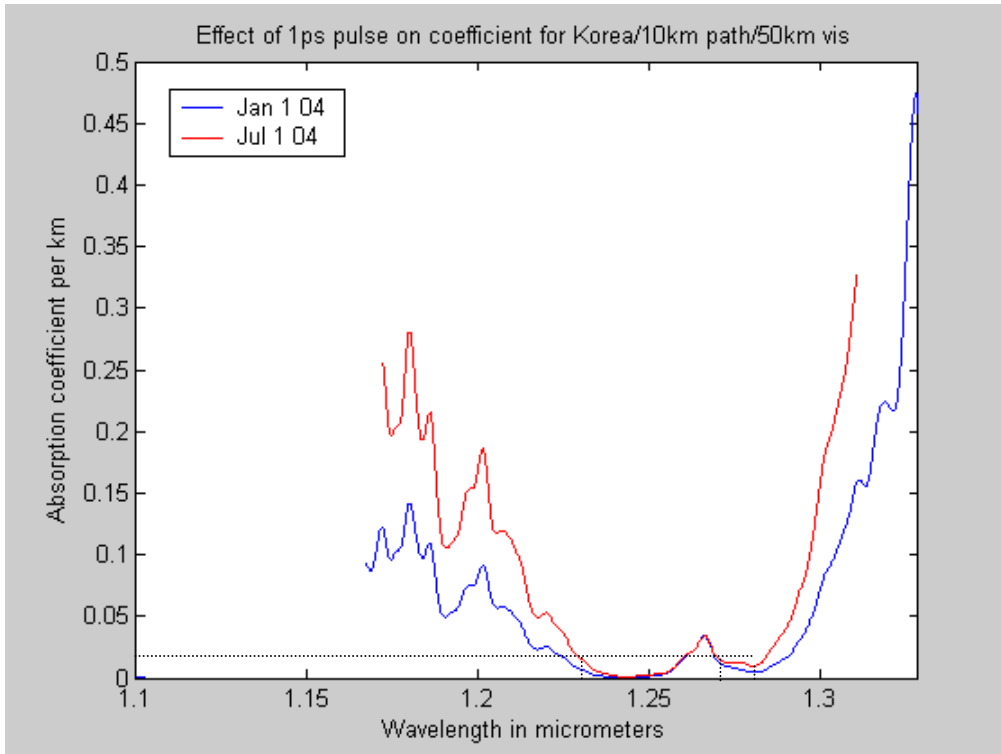


Figure 33. Absorption coefficient for a 1 ps FEL Gaussian pulse from 1.11 to 1.33 μm using FASCODE for a 10 km long, 10 m high path for Korea on 1 Jan and 1 July.

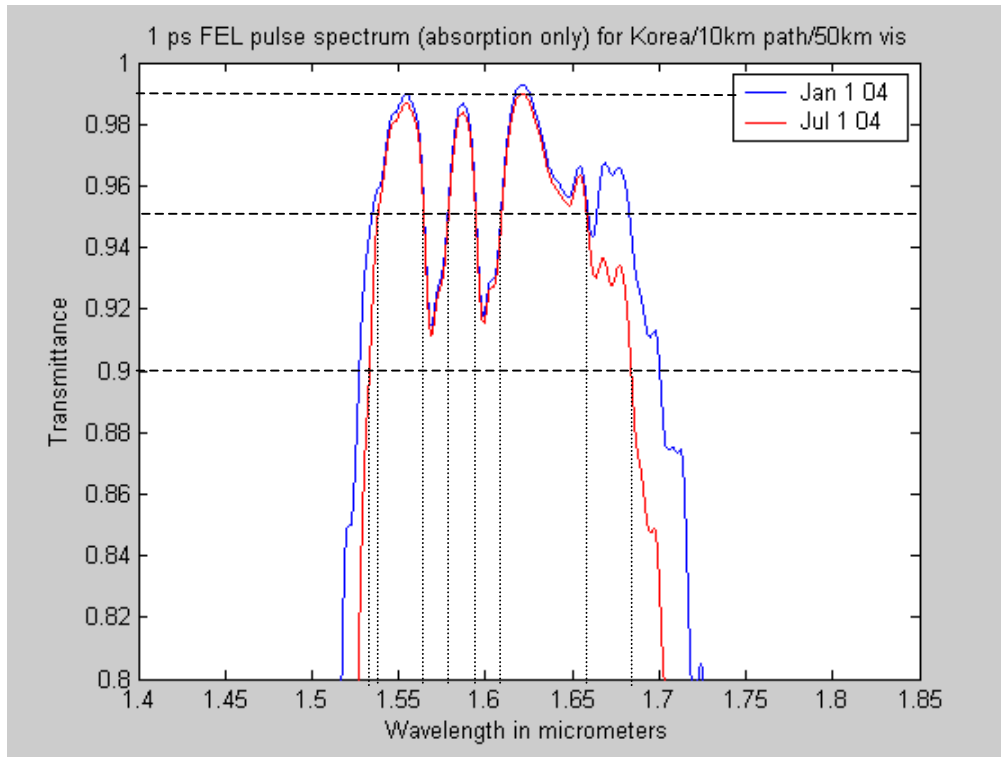


Figure 34. Molecular transmission for a 1 ps FEL Gaussian pulse from 1.47 to 1.82 μm using FASCODE for a 10 km long, 10 m high path for Korea on 1 Jan and 1 July.

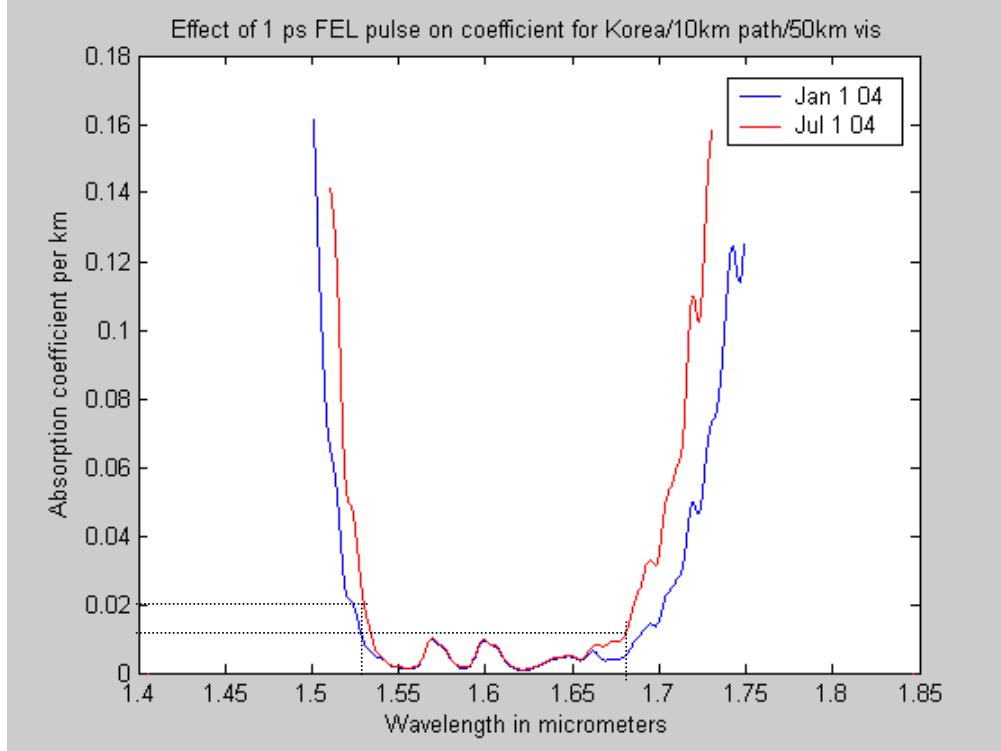


Figure 35. Absorption coefficient for a 1 ps FEL Gaussian pulse from 1.47 to 1.82 μm using FASCODE for a 10 km long, 10 m high path for Korea on 1 Jan and 1 July.

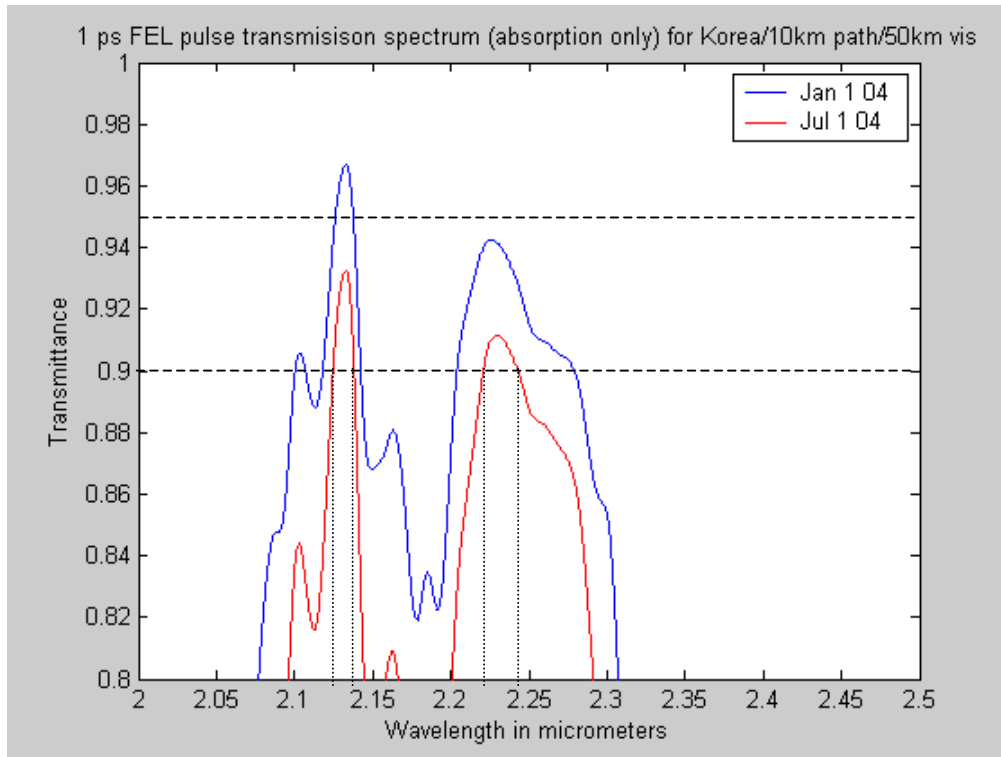


Figure 36. Molecular transmission for a 1 ps FEL Gaussian pulse from 2 to 2.5 μm using FASCODE for a 10 km long, 10 m high path for Korea on 1 Jan and 1 July.

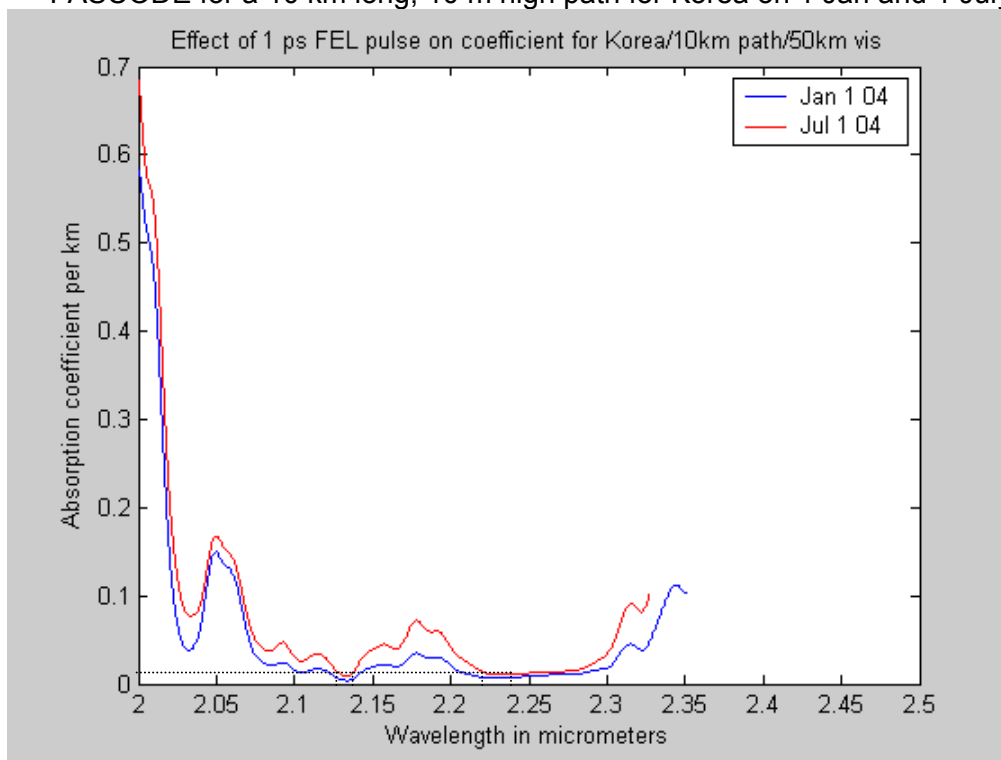


Figure 37. Absorption coefficient for a 1 ps FEL Gaussian pulse from 2 to 2.5 μm using FASCODE for a 10 km long, 10 m high path for Korea on 1 Jan and 1 July.

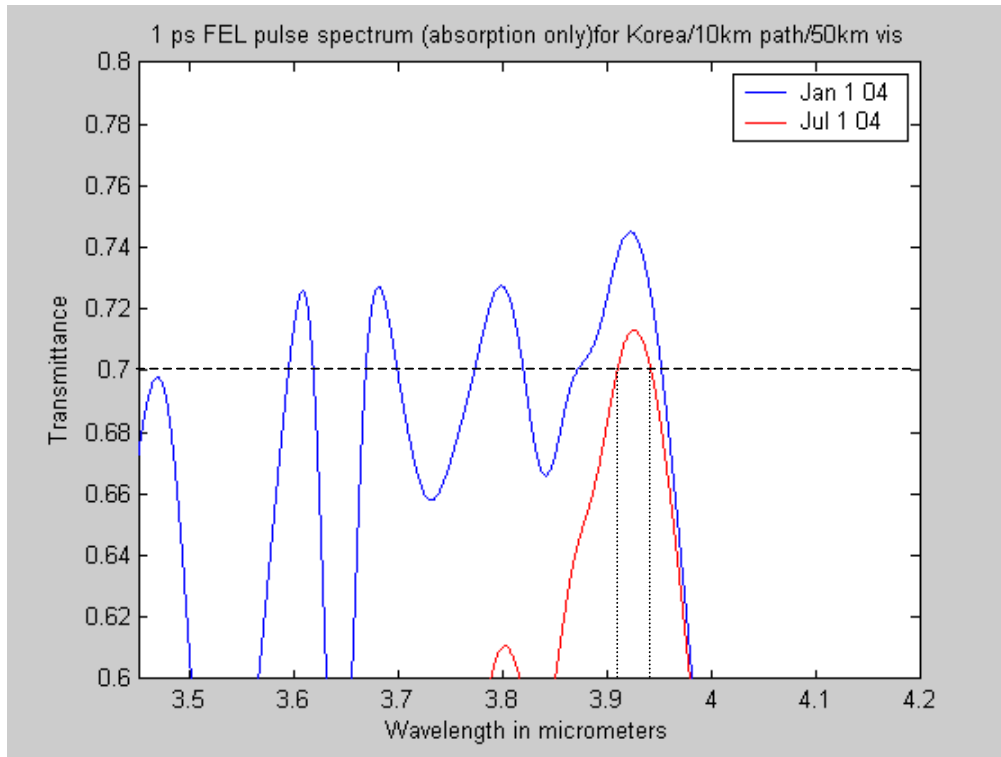


Figure 38. Molecular transmission for a 1 ps FEL Gaussian pulse from 3.45 to 4.16 μm using FASCODE for a 10 km long, 10 m high path for Korea on 1 Jan and 1 July.

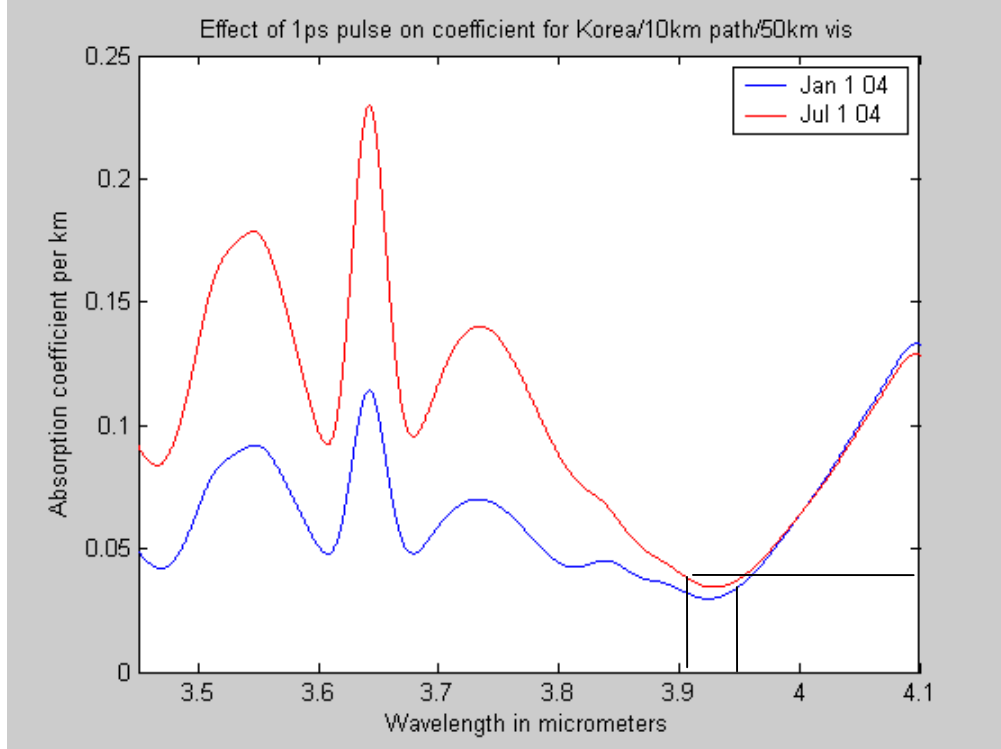


Figure 39. Absorption coefficient for a 1 ps FEL Gaussian pulse from 3.45 to 4.16 μm using FASCODE for a 10 km long, 10 m high path for Korea on 1 Jan and 1 July.

H. MODTRAN AND FASCODE CONSISTENCY

This section of the thesis work compares the results from MODTRAN and FASCODE. Since HITRAN data is used as a direct input to FASCODE and indirect input to MODTRAN, we would expect the results of FASCODE and MODTRAN to be quite close. Figures 38 to 42 show the plots of the selected five wavelength bands of interest. In general, the MODTRAN and FASCODE results are very similar, except around the 1.05 to 1.07 μm and 1.23 to 1.28 μm bands whereby the difference is the greatest with MODTRAN having lower transmittance values than FASCODE by about 10%. This observation shows that MODTRAN can be used as a good approximation to FASCODE results with the advantages of faster computational time and larger spectral band per run. However, it should be noted that MODTRAN does not give accurate results for higher altitude atmospheric paths (above 60 km) band modeling and should be used with caution.

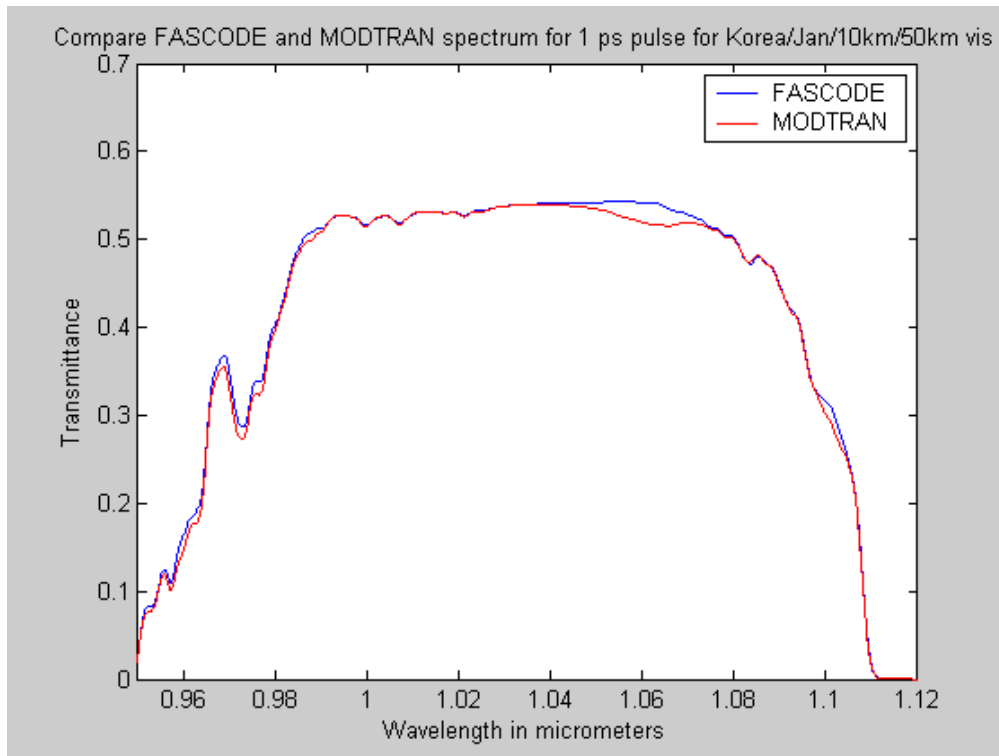


Figure 40. FASCODE and MODTRAN spectra for a 1 ps FEL Gaussian pulse from 0.95 to 1.12 μm for a 10 km long, 10 m high path with 50 km visibility for Korea on 1 Jan.

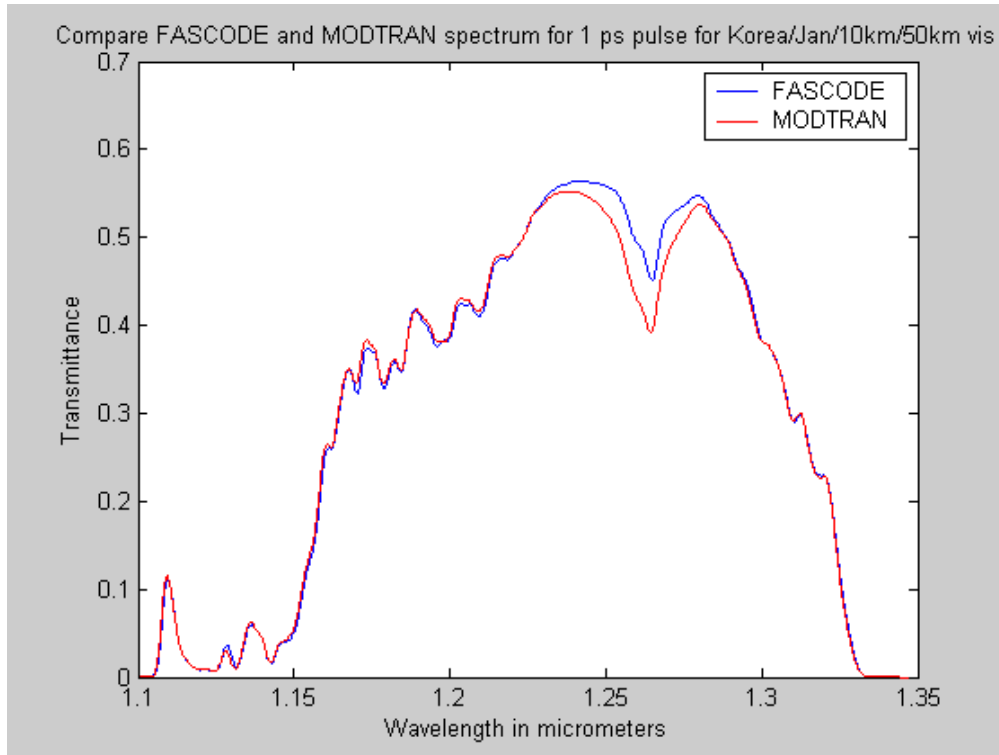


Figure 41. FASCODE and MODTRAN spectra for a 1 ps FEL Gaussian pulse from 1.1 to 1.35 μm for a 10 km long, 10 m high path with 50 km visibility for Korea on 1 Jan.

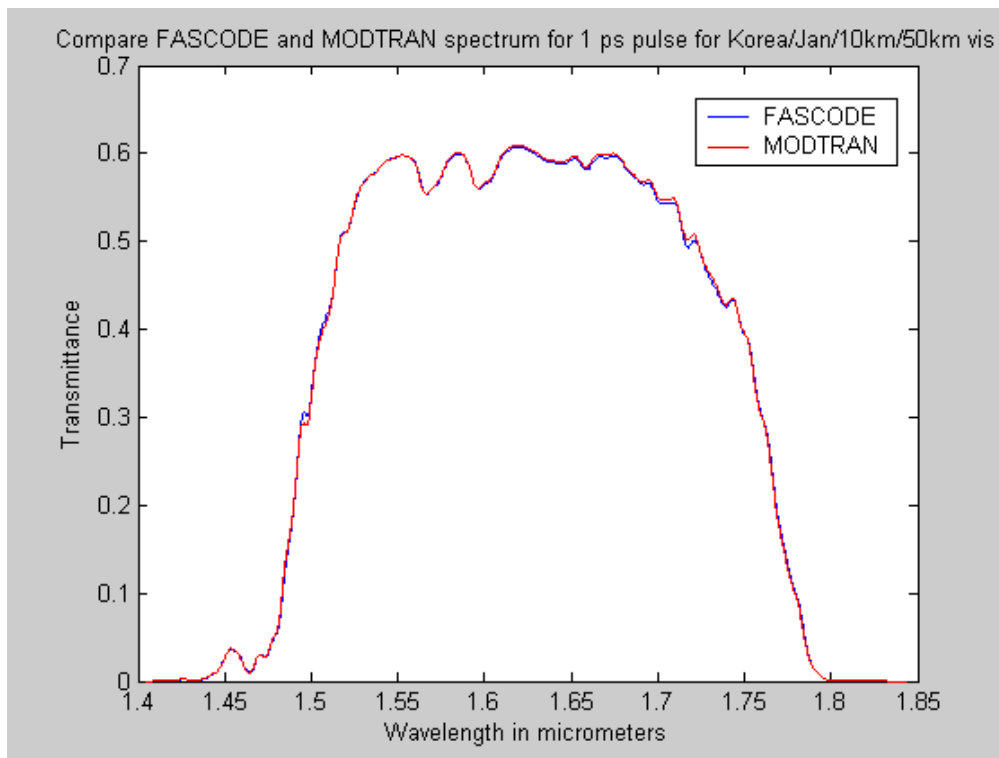


Figure 42. FASCODE and MODTRAN spectra for a 1 ps FEL Gaussian pulse from 1.4 to 1.85 μm for a 10 km long, 10 m high path with 50 km visibility for Korea on 1 Jan.

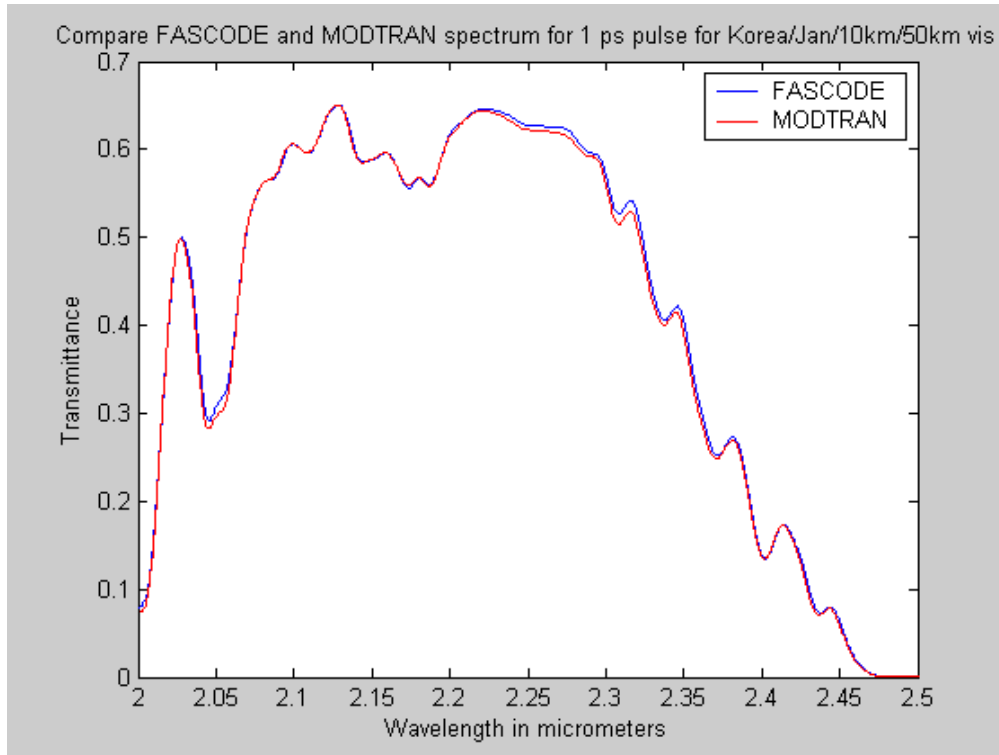


Figure 43. FASCODE and MODTRAN spectra for a 1 ps FEL Gaussian pulse from 2 to 2.5 μm for a 10 km long, 10 m high path with 50 km visibility for Korea on 1 Jan.

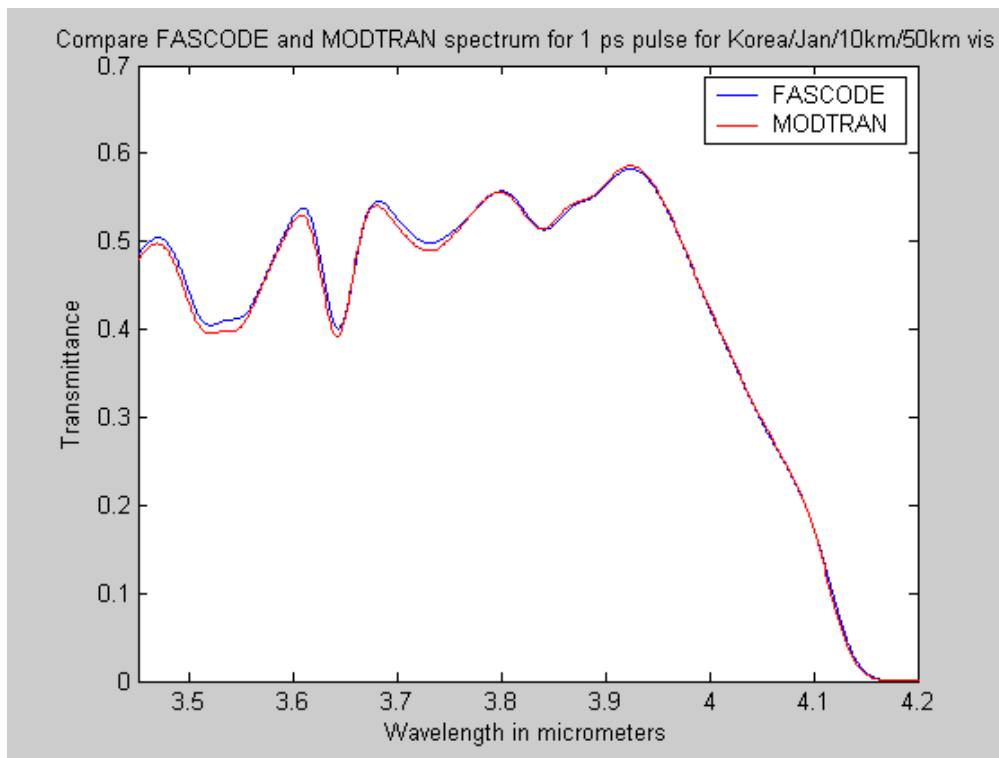


Figure 44. FASCODE and MODTRAN spectra for a 1 ps FEL Gaussian pulse from 3.45 to 4.2 μm for a 10 km long, 10 m high path with 50 km visibility for Korea on 1 Jan.

I. EFFECTS OF LONGER PULSE WIDTHS

We have seen in section D of this chapter that increasing the FEL pulse width has the effect of decreasing the spectral width. Thus far, most of the simulation runs have used a 1 ps pulse width as the reference. Pulse width of 0.25 and 1 ps were compared earlier in Figure 14. It would be useful to know what pulse length is required so that the laser spectrum is narrow enough to be able to squeeze between the molecular absorption lines.

Figures 43 to 45 show the comparison of transmission spectra for 2, 5 and 10 ps pulse widths with the 1 ps FEL pulse. Pulse widths of 5 ps and larger are able to fit between the atmospheric absorption peaks but as the pulse width increased, the values of the local maxima of the spectrum increased while the local minima decreased.

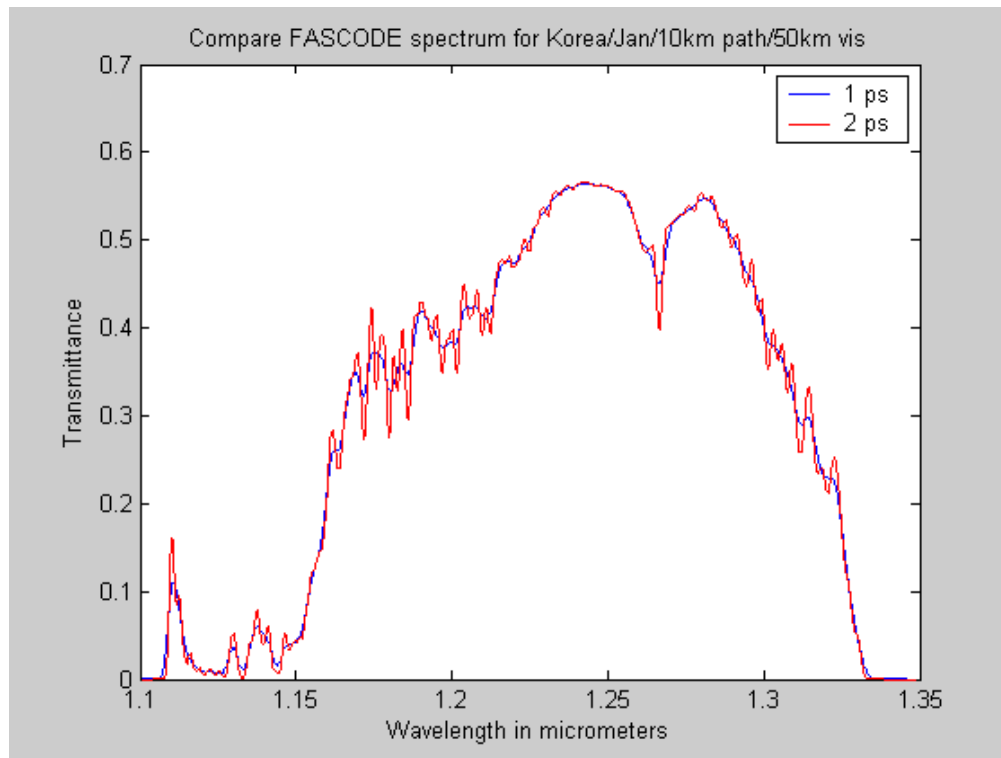


Figure 45. Atmospheric extinction spectra between 1.1 and 1.35 μm for 1 ps and 2 ps Gaussian pulses for a 10 km long, 10 m high path for Korea on 1 Jan.

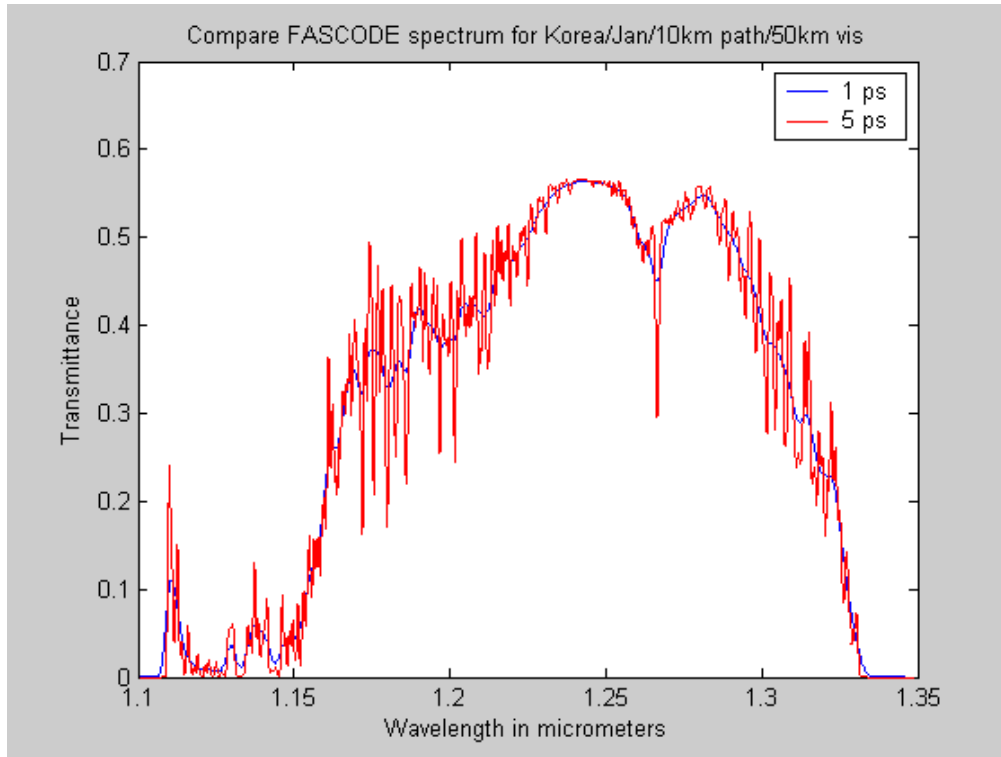


Figure 46. Atmospheric extinction spectra between 1.1 and 1.35 μm for 1 ps and 5 ps Gaussian pulses for a 10 km long, 10 m high path for Korea on 1 Jan.

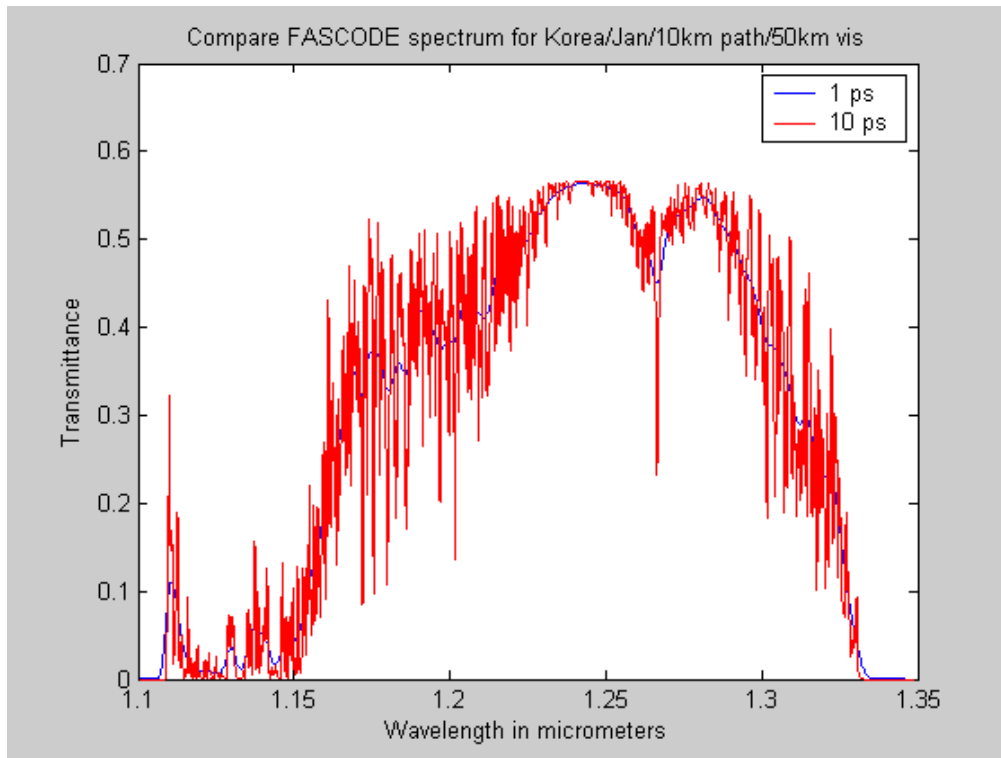


Figure 47. Atmospheric extinction spectra between 1.1 and 1.35 μm for 1 ps and 10 ps Gaussian pulses for a 10 km long, 10 m high path for Korea on 1 Jan.

Increasing the pulse width has the same effect on the absorption coefficient spectrum; i.e., peak values of the spectrum increase with increasing pulse width while the trough values decrease. (See Figures 48 to 50). The results show that operating a longer pulse FEL weapon requires careful selection of optimal wavelengths as it is more sensitive to wavelength because its narrower spectral width can encounter or avoid the atmospheric absorption features. Choosing the right wavelength for a longer pulse offers the advantage of exploiting narrow, low absorption windows and hence better transmittance of laser energy and delivery of higher power onto the target compared to a shorter pulse laser operating on the same wavelength. However, the effects of laser pulsewidth are less important near the regions of lowest absorption such as around the 1.24 μm band in Figures 48 to 50.

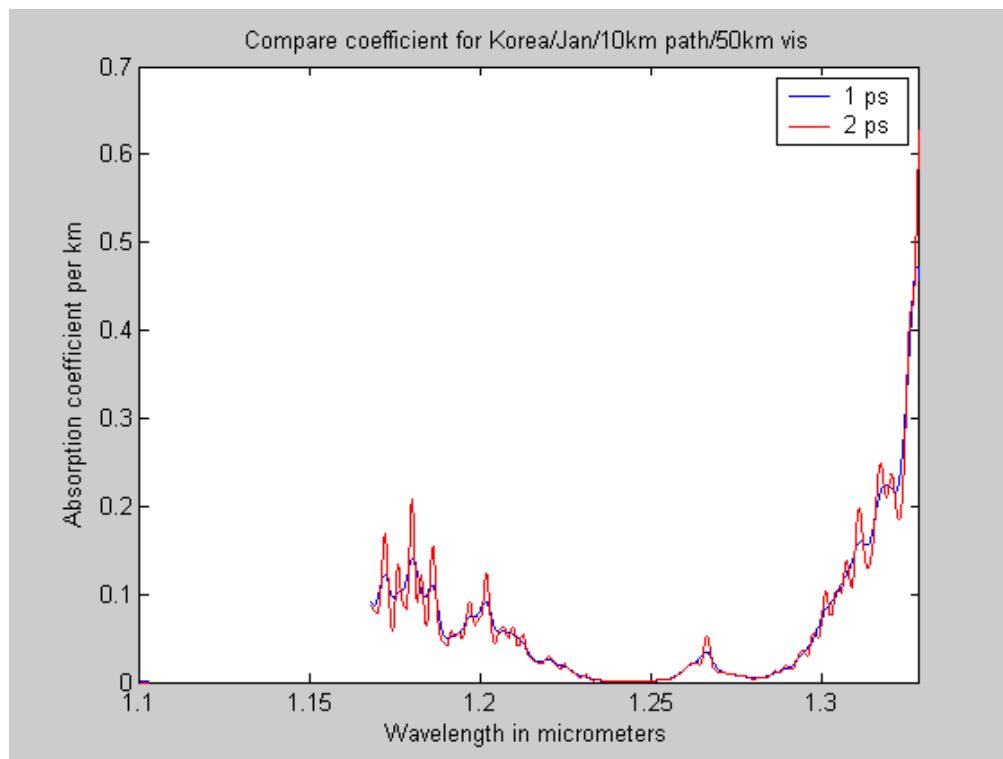


Figure 48. FASCODE absorption coefficients convolved with 1 and 2 ps Gaussian pulses for a 10 km long, 10 m high path for Korea on 1 Jan.

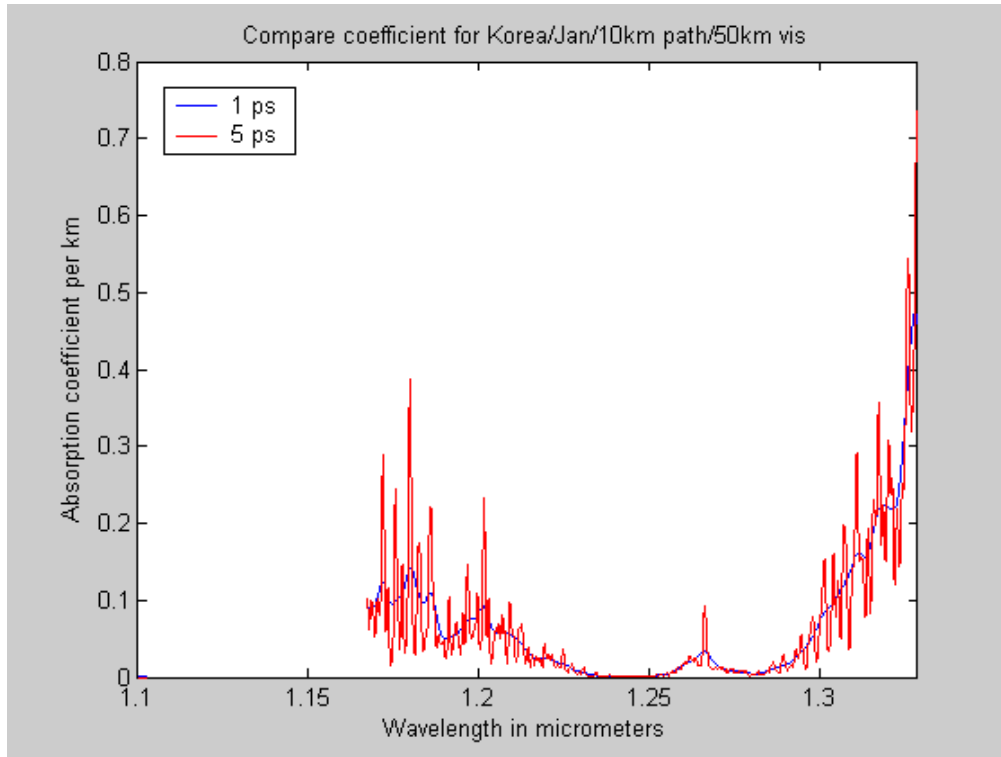


Figure 49. FASCODE absorption coefficients convolved with 1 and 5 ps Gaussian pulses for a 10 km long, 10 m high path for Korea on 1 Jan.

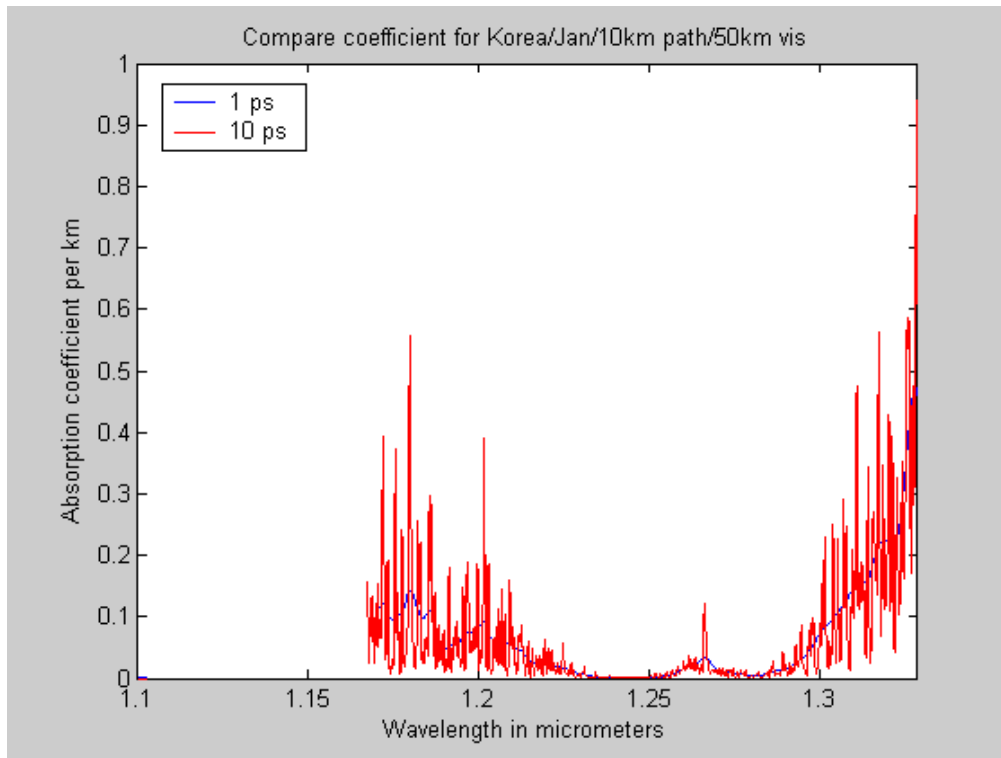


Figure 50. FASCODE absorption coefficients convolved with 1 and 10 ps Gaussian pulses for a 10 km long, 10 m high path for Korea on 1 Jan.

V. CONCLUSIONS AND RECOMMENDATIONS

A. CONCLUSIONS

The possibility of using a laser beam as a ship-borne self-defense weapon has become more feasible with recent advancements in laser technology. The advantages of a high energy laser as a weapon are its key attributes of speed-of-light response, ability to handle fast maneuvering and crossing targets, deep magazine capacity, minimal collateral damage, target identification and adaptability for lethal to non-lethal employment. The attenuation of laser energy by the atmosphere is a result of molecular attenuation and scattering. Atmospheric scattering mainly disperses the energy of the laser beam but molecular absorption heats the atmosphere, reducing the index of refraction and thereby creating thermal blooming. The FEL has potential as a shipborne weapon system because it can be designed to operate at any desired frequency and, to a degree, is tunable in operation. The ability to select an operating frequency greatly enhances the successful propagation of the laser beam through the relatively dense air at low altitudes.

The objective of this thesis was to determine optimal operating wavelength bands for a high energy FEL weapon between 0.6 μm and 4.2 μm using the US Air Force PLEXUS Release 3 Version 2 program to set up MODTRAN 4 Version 2 and FASCODE 3 atmospheric transmission programs. Since PLEXUS and its user interface are export limited, this thesis was restricted to processing the MODTRAN and FASCODE output files. These codes allow for complex atmospheric transmittance and radiance calculations based on absorption and scattering phenomena for a variety of path geometries. The input parameters chosen for the simulation runs are meant to represent likely operational scenarios for ship self defense against a cruise missile attack. The main consideration was a 10 m altitude horizontal transmission path. Korea, Taiwan

and the Persian Gulf were the three geographical areas chosen for the study. The effect of a short FEL laser pulse was modeled by convolving a normalized Gaussian frequency spectrum with the MODTRAN and FASCODE transmission and absorption coefficient spectra. The result of the convolution operation averages the transmittance values over a number of wavenumbers. The amount of averaging increases as the length of the FEL pulse decrease.

A comparison of the FASCODE and MODTRAN spectra shows close correlation for the input parameters chosen for this study, and suggests that MODTRAN results are suitable for use as estimations to the FASCODE runs, except around 1.06 and 1.26 μm .

1. MODTRAN Results

Initial runs were carried out with the 1 cm^{-1} resolution MODTRAN 4.0 program. Five atmospheric windows occur between 0.95 and 1.1 μm , 1.2 to 1.33 μm , 1.47 to 1.82 μm , 2 to 2.5 μm and 3.5 to 4 μm . For a 50 km visibility, the transmission in the five atmospheric windows drops from around 90% for a 2 km path to 50% for a 10 km path. Aerosol extinction is the dominant source of loss in these windows and the effects increase at shorter wavelengths reducing the transmission to 60% at 2 μm and 50% at 1 μm for the 10 km path. The transmission spectra do not vary much with geographical location or season except in the 3.5 to 4 μm band when warmer seasons or locations increase the amount of water vapor and reduce the transmission by 30%. Changing the laser pulse length varies the amount of averaging of the transmission spectra. The transmission spectra for pulse widths of 0.25 to 1 ps are similar. Pulse lengths of 5 ps and longer were able to slip between or hit individual atmospheric absorption lines, particularly at the edges of the atmospheric windows. There was little improvement for longer pulses at the lowest absorbing regions.

2. FASCODE Results

The higher resolution 0.1 cm^{-1} FASCODE was used to conduct further analysis on five selected bands or “windows” found from the MODTRAN results. Using the FASCODE aerosol extinction output file results, absorption coefficients for each wavenumber (or spectral frequency) were calculated. The molecular absorption coefficient is a key parameter for thermal blooming calculations. Data for the absorption coefficient were also used to compute the transmission spectrum for molecular absorption only. Using the transmission spectrum and absorption coefficient graphs, the optimal wavelength bands for employment of FEL at low altitudes were identified and summarized in Table 5. The four main bands of 0.95 to 1.11 μm , 1.11 to 1.33 μm , 1.47 to 1.82 μm , and 2 to 2.5 μm contain quite a number of suitable wavelengths that allow transmittance of at least 90% for a 10 km path and have absorption coefficient values of 0.02 per km or less. For a more stringent requirement of at least 99% transmittance, the suitable wavelength windows are between 1.03 to 1.06 μm and around 1.241 and 1.624 μm . However, the main concern for laser transmission through the atmosphere in the 1 μm region is the strong aerosol extinction.

B. RECOMMENDATIONS FOR FURTHER WORK

The fidelity of the simulation results depends on the accuracy of the environment and aerosol model used for the simulation runs. The primary analysis in this study considered the molecular absorption component of the atmosphere. Aerosol scattering has a strong effect at the higher frequencies and the extinction around 1 to 2 μm depends on the size distribution of the aerosol. The aerosol model is subjective and depends on the perceived visibility conditions with an assumed size distribution that depends on wind speed and humidity. Future work to improve the assessment of optimal operating frequencies should include verifying the accuracy or replacing the Navy Aerosol

model that is used in both MODTRAN and FASCODE programs, in particular the relationship between visibility range and aerosol concentration. The availability of actual aerosol concentration data and visibility histograms from the geographical areas of interest are essential for a more complete and robust assessment of the actual transmission of laser energy through the atmosphere.

LIST OF REFERENCES

- [1] Elihu Zimet, "High Energy Lasers: Technical, Operational, and Policy Issues", Defense Horizons, October 2002.
- [2] H.P. Freund and T.M. Antonsen Jr, "Principles of Free-electron Lasers," Chapman and Hall, 1996.
- [3] Frederick G. Gebhardt, High Power Laser Propagation, Applied Optics, Vol.15, No.6, June 1976.
- [4] Michael E. Thomas & Donald D. Duncan, "Atmospheric Transmission", The Infrared & Electro-Optical Systems Handbook, Volume 2: Atmospheric Propagation of Radiation, SPIE Press, 1996.
- [5] J.H. Shaw, Ohio J. Sci. 53, 258, 1953.
- [6] A.W. Cooper, Notes from PH 4253 Course, Naval Postgraduate School, Monterey, California, September 1998.
- [7] William L. Wolfe and George J. Zissis, "The Infrared Handbook", The Infrared Information and Analysis Center, Environmental Research Institute of Michigan, 1978.
- [8] K.E. Woehler, "Directed Energy Weapon Concepts, Part 1" Course Notes, Naval Postgraduate School, Monterey, California, Spring 2002.
- [9] Gerald C. Holst, Electro-Optical Imaging System Performance, Third Edition, SPIE Press, JCD Publishing, 2003.
- [10] B.W. Rice and G.A. Findlay, "Infrared Propagation Within a Few meters of the Sea Surface," Applied Optics, 29(34), 1990.
- [11] C.R. Zeisse, "NAM6: Batch Code for the Navy Aerosol Model", Technical report 1804, Office of Naval Research, United States Navy, October 1999.
- [12] A.D. Devir, A. Ben-Shalom et al, "Experimental validation of atmospheric transmittance codes", Optical, Infrared, and Millimeter-Wave

Propagation Engineering, W.B. Miller and N.S. Kopeika, Eds., Proc. SPIE 926, 54-64, 1988.

[13] G.P. Anderson, et al., 1995, Passive Infrared Remote Sensing of Clouds and the Atmosphere II, David K. Lynch, Editor, Proc. SPIE 2309, 170-183, 1994.

[14] Frank L. Pedrotti and Leno S. Pedrotti, "Introduction to Optics", 2nd Edition, Prentice Hall, 1993.

[15] Martin A Pollack, Robert J. Pressley (Editor), "Handbook of Lasers with Selected Data on Optical Technology", The Chemical Rubber Co, Ohio, 1971.

INITIAL DISTRIBUTION LIST

1. Defense Technical Information Center
Ft. Belvoir, Virginia
2. Dudley Knox Library
Naval Postgraduate School
Monterey, California
3. Professor Donald L. Walters, Code Ph/We
Department of Physics
Monterey, California
4. Professor Alfred W. Cooper, Code Ph/Cr
Department of Physics
Monterey, California
5. CAPT Roger McGinnis
Naval Sea Systems Command
Washington, D.C.
6. Chairman, Physics Department, Code Ph/Lj
Naval Postgraduate School
Monterey, California
7. Physics Department (Code Ph)
Naval Postgraduate School
Monterey, California
8. Director, Temasek Defence Systems Institute
Professor Yeo Tat Soon
Block E1, #05-05
Singapore